



**HAL**  
open science

## Ion temperature gradient mode mitigation by energetic particles, mediated by forced-driven zonal flows

J N Sama, A. Biancalani, A. Bottino, D. Del Sarto, R J Dumont, Giovanni Di Giannatale, A. Ghizzo, T. Hayward-Schneider, Ph. Lauber, B. Mcmillan, et al.

### ► To cite this version:

J N Sama, A. Biancalani, A. Bottino, D. Del Sarto, R J Dumont, et al.. Ion temperature gradient mode mitigation by energetic particles, mediated by forced-driven zonal flows. *Physics of Plasmas*, 2024, 31 (11), pp.112503. 10.1063/5.0226833 . hal-04763379

**HAL Id: hal-04763379**

**<https://hal.science/hal-04763379v1>**

Submitted on 1 Nov 2024

**HAL** is a multi-disciplinary open access archive for the deposit and dissemination of scientific research documents, whether they are published or not. The documents may come from teaching and research institutions in France or abroad, or from public or private research centers.
















L'archive ouverte pluridisciplinaire **HAL**, est destinée au dépôt et à la diffusion de documents scientifiques de niveau recherche, publiés ou non, émanant des établissements d'enseignement et de recherche français ou étrangers, des laboratoires publics ou privés.



Distributed under a Creative Commons Attribution 4.0 International License

RESEARCH ARTICLE | NOVEMBER 01 2024

## Ion temperature gradient mode mitigation by energetic particles, mediated by forced-driven zonal flows

J. N. Sama ; A. Biancalani ; A. Bottino ; D. Del Sarto ; R. J. Dumont ; G. Di Giannatale ; A. Ghizzo ; T. Hayward-Schneider ; Ph. Lauber; B. McMillan ; A. Mishchenko ; M. Muruggapan ; B. Rettino; B. Rofman ; F. Vannini ; L. Villard ; X. Wang 



*Phys. Plasmas* 31, 112503 (2024)

<https://doi.org/10.1063/5.0226833>



### Articles You May Be Interested In

Transforming underground to surface mining operation – A geotechnical perspective from case study

*AIP Conference Proceedings* (November 2021)

Monthly prediction of rainfall in nickel mine area with artificial neural network

*AIP Conference Proceedings* (November 2021)

Estimation of Karts groundwater based on geophysical methods in the Monggol Village, Saptosari District, Gunungkidul Regency

*AIP Conference Proceedings* (November 2021)



Physics of Plasmas

Special Topics Open  
for Submissions

[Learn More](#)

# Ion temperature gradient mode mitigation by energetic particles, mediated by forced-driven zonal flows

Cite as: Phys. Plasmas **31**, 112503 (2024); doi: [10.1063/5.0226833](https://doi.org/10.1063/5.0226833)

Submitted: 4 July 2024 · Accepted: 15 October 2024 ·

Published Online: 1 November 2024



View Online



Export Citation



CrossMark

J. N. Sama,<sup>1,a)</sup> A. Biancalani,<sup>2</sup> A. Bottino,<sup>3</sup> D. Del Sarto,<sup>1</sup> R. J. Dumont,<sup>4</sup> G. Di Giannatale,<sup>5</sup> A. Ghizzo,<sup>1</sup> T. Hayward-Schneider,<sup>3</sup> Ph. Lauber,<sup>3</sup> B. McMillan,<sup>6</sup> A. Mishchenko,<sup>7</sup> M. Muruggapan,<sup>5</sup> B. Rettino,<sup>3</sup> B. Rofman,<sup>5</sup> F. Vannini,<sup>3</sup> L. Villard,<sup>5</sup> and X. Wang<sup>3</sup>

## AFFILIATIONS

<sup>1</sup>Université de Lorraine, CNRS, IJL, 54011 Nancy, France

<sup>2</sup>Léonard de Vinci Pôle Universitaire, Research Center, 92400 Paris La Défense, France

<sup>3</sup>Max Planck Institute for Plasma Physics, 85748 Garching, Germany

<sup>4</sup>CEA, IRFM, F-13108 Saint-Paul-lez-Durance, France

<sup>5</sup>Swiss Plasma Center, EPFL, 1015 Lausanne, Switzerland

<sup>6</sup>Center for Fusion, Space and Astrophysics, University of Warwick, Coventry CV4 7AL, United Kingdom

<sup>7</sup>Max Planck Institute for Plasma Physics, 17491 Greifswald, Germany

<sup>a)</sup> Author to whom correspondence should be addressed: [juvert-njeck.sama@univ-lorraine.fr](mailto:juvert-njeck.sama@univ-lorraine.fr)

## ABSTRACT

In this work, we use the global electromagnetic and electrostatic gyro kinetic approaches to investigate the effects of zonal flows forced-driven by Alfvén modes due to their excitation by energetic particles on the dynamics of ITG (ion temperature gradient) instabilities. The equilibrium of the 92416 JET tokamak shot is considered. The linear, nonlinear Alfvén modes, and the zonal flow dynamics are investigated, and their respective radial structures and saturation levels are reported. ITG dynamics in the presence of the zonal flows excited by these Alfvén modes are also investigated. The zonal flows forced-driven by Alfvén modes can significantly impact the ITG dynamics. A zonal flow amplitude scan reveals the existence of an inverse relation between the zonal flow amplitude and the ITG growth rate. These results indicate that forced-driven zonal flows can be an important indirect part of turbulence mitigation due to the injection of energetic particles.

© 2024 Author(s). All article content, except where otherwise noted, is licensed under a Creative Commons Attribution (CC BY) license (<https://creativecommons.org/licenses/by/4.0/>). <https://doi.org/10.1063/5.0226833>

## I. INTRODUCTION

### A. Motivations

Drift wave turbulence and its associated heat and particle transport have been intensively studied due to their role in deteriorating plasma confinement, which is a concern for future fusion plasma reactors. The ion-temperature gradient modes (ITG) are drift waves driven unstable by the ion-temperature gradient. The spontaneous nonlinear excitation of zonal flows by ITG modes,<sup>1–3</sup> is believed to be one of their major saturation mechanisms. Zonal flows (ZF), i.e., axisymmetric perturbations of tokamak plasmas, play an important role in the self-consistent turbulence saturation. There are two types: the zero frequency zonal flow (ZFZF) and the finite frequency geodesic acoustic modes (GAMs).<sup>4–7</sup> The ZFZF can be generated by ITGs and their lower frequency branch, in which only ions trapped in the banana

orbits intervene.<sup>8–12</sup> Trapped ion modes (TIM) is the name given to this lower frequency branch of ITGs (an electron counterpart also exists). The turbulence and ZFZF generated by the high-frequency branch of ITGs are generally dominant over those generated by the TIMs. Due to thermal species non-linearity, the Reynolds stress dominates the ZFZF dynamics in electrostatic drift wave turbulence.<sup>13</sup> Other studies suggest that the zonal flow dynamics are governed by the competition between the Reynolds and diamagnetic stresses.<sup>14</sup> The contribution of the Maxwell stress has also been reported in electromagnetic regimes.<sup>15</sup> However, we focus on zonal flows excited by Alfvén modes, whose dynamics are dominated by the contributions of energetic particles to the curvature coupling term in the vorticity equation.<sup>16</sup> A conjecture by Biancalani *et al.*<sup>17</sup> claims zonal flows excited by Alfvén modes can be used to mitigate background ITG turbulence. In

this study, we design numerical simulations to test this claim by investigating the role of forced-driven zonal flows excited by linearly unstable fast ion modes on ITG instabilities.

## B. Historical context and state of the art

Various operational regimes have been observed in tokamaks, such as JET, AUG, and DIII-D. These regimes include the low confinement regime (L-mode) and the high confinement regime (H-mode). The transition from L-mode to H-mode is characterized by a significant reduction in transport and the creation of an edge transport barrier (ETB).<sup>18</sup> Over the past few decades, extensive research has been conducted on developing the advanced tokamak scenario, including the Internal Transport Barrier (ITB),<sup>19–22</sup> and on the study of the impact of fast particles<sup>21,23–25</sup> on turbulence and transport. Garcia *et al.*<sup>26</sup> provide an extensive overview of fast particles' role in transport mitigation and turbulence, and more recently, Citrin *et al.*<sup>20</sup> also reviewed this topic. Three mechanisms have been identified in the literature to be responsible for transport mitigation by fast particles, i.e., thermal ion dilution,<sup>22,27</sup> electrostatic stabilization of micro-instabilities by the resonant interaction of fast particles with waves<sup>28,29</sup> and electromagnetic stabilization.<sup>30–34</sup> Analysis of local flux-tube simulations explains nonlinear electromagnetic stabilization effects by the presence of marginally stable fast particle modes which are nonlinearly excited and act as a mediator of turbulence suppression by zonal flows. These simulations also reveal that in the presence of linearly unstable fast ion modes, transport reduction via electromagnetic stabilization by fast particles would not be active.<sup>26,35</sup> According to a recent study by Di Siena *et al.*,<sup>36</sup> which compared local flux-tube and global gyrokinetic simulations of fast particle effects on core turbulence, the local flux-tube simulations were found to qualitatively reproduce the global results only in the electrostatic and marginally stable regimes. The study reports that the local simulations overestimated the energetic particle turbulence stabilization by approximately 40% for the marginally stable case, while the local approximation was inadequate to accurately model turbulent fluxes in plasma regimes with linearly unstable energetic particle-driven modes.

A recent JET experiment destabilized various Alfvén eigenmodes during ICRH heating, resulting in improved confinement of thermal ions.<sup>37,38</sup> This stabilization is believed to be due to an interplay between turbulence, Alfvén modes, and zonal flows. However, the exact source of these zonal flows and the role played by energetic particles remains an open question. Several analytical theories and models<sup>39–43</sup> have been developed in the last few decades and numerical flux-tube simulations performed.<sup>20,34,44–47</sup> Qiu and coworkers<sup>16</sup> proposed a theoretical model in which zonal flows can be driven by linearly unstable Alfvén modes (AM)<sup>48,49</sup> in the presence of energetic particles (marginally stable fast ion modes cannot drive zonal flows via this mechanism). According to their model, the energetic particles' nonlinearity that enters the vorticity equation through the curvature coupling term dominates over the bulk particles' non-linearity associated with the Reynolds and Maxwell stresses responsible for the excitation of zonal flows by drift waves. Under this condition, the Alfvén modes can drive a zonal flow with a growth rate that is twice that of the Alfvén modes. The zonal flows excited by this mechanism are termed to be forced-driven. There exists no amplitude threshold for forced-driven zonal flow excitation by AM. Zonal flows forced driven by Alfvén modes were first observed in simulation by Todo.<sup>50</sup>

Recently, global simulations with the gyro-kinetic particle-in-cell code ORB5<sup>51,52</sup> have been performed, where the self-consistent interaction of ITG turbulence, zonal flows, and Alfvén modes has been studied in the presence of energetic particles.<sup>17,53</sup> Similar studies have been made with other codes.<sup>54,55</sup> The work done by Biancalani *et al.*<sup>17</sup> on the self-consistent interaction of energetic particles, Alfvén modes, and zonal flows provides, in particular, the main motivation for the present study. It is, therefore, useful to first recall the main results of that work to better put it in context and highlight the scope of the present manuscript. In Ref. 17, a circular concentric magnetic equilibrium was used to perform self-consistent electromagnetic turbulence simulations with global gyrokinetic particles in cell code ORB5. These simulations consisted of two phases. In the first phase, the simulation setup was such that ITG modes were driven unstable by the temperature gradient of the main ion species. The energetic particle species was small in comparison and was configured with a flat temperature profile with a value equivalent to that of the main ion species at the location where the gradient of the ion species admits its maximum value. Energetic particles configured in this way act just like ordinary bulk ions. With these configurations, the simulation was launched with the toroidal mode number in the interval  $\{0, 40\}$ . The linear growth phase of the mode is dominated by the toroidal mode in the interval  $\{20, 30\}$ , with the fastest growing mode being  $n = 25$ , the corresponding figure shown in Ref. 17 is reproduced next as Fig. 1, for convenience. This linear phase was followed by a nonlinear saturation phase in which zonal flows (mode with  $n = 0$ ) were self-consistently driven by the resulting ITG turbulence, which was self-consistently described by the nonlinear code ORB5. It is here that a “second stage” of the numerical experiment of Ref. 17 can be identified: the simulation was stopped

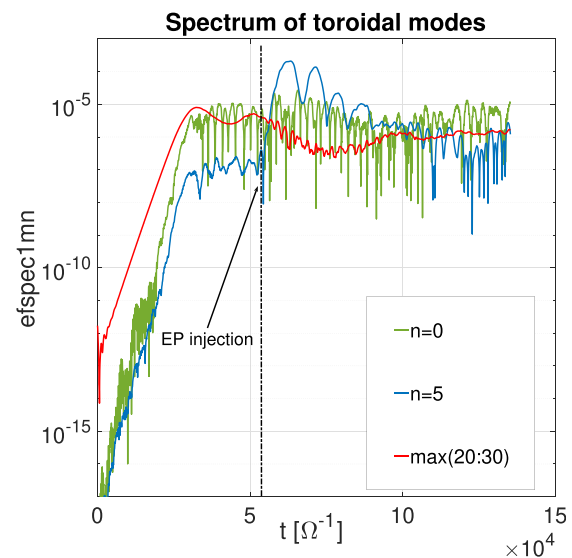


**FIG. 1.** Plot of the time evolution of the field energy (efspec1mn) from ORB5 global electromagnetic simulation performed by the authors in Ref. 17. Time is in units of the inverse ion cyclotron frequency  $\Omega_i^{-1}$  and field energy in units of the electron temperature. Red curve sum of field energies of ITG mode in the range  $n = \{20, 30\}$ . The blue curve represents the  $n = 5$  Alfvén mode, and the Green curve represents the zonal flow. The dotted black line represents the time at which the energetic particles are injected. This plot has been adapted from Ref. 17, with the authors' permission.

deep into the nonlinear phase, and the energetic particles were activated by setting their temperature to a value 10 times the value of the bulk ion temperature. This was done so to specifically study the effect that a population of energetic particles would have on the self-consistently generated ITG turbulence. A restart of the same simulation was thus made with the energetic particles activated (restart from the dotted black line in Fig. 1). It was then observed that energetic particles excited an Alfvén eigenmode on the background ITG turbulence, and this was followed by a significant increase in the zonal flow levels. The excitation of the Alfvén mode and zonal flow led to a reduction of fluctuation levels of the background ITG turbulence level (red curve of Fig. 1 in the interval  $[52\,000, 70\,000]\Omega_i^{-1}$ ) by roughly an order of magnitude.

These results indicate a possible relationship between zonal flow excitation by unstable Alfvén modes and background turbulence mitigation. However, ascertaining in a self-consistent framework if the stabilization of the background turbulence is precisely due to the action of these zonal flows is a challenging problem. This is due to the complex nonlinear nature of the problem of the self-consistent interaction of turbulence, Alfvén modes, and zonal flows. A multitude of nonlinear effects have been reported in the related literature and have been shown to contribute to the mitigation of drift wave turbulence (e.g., thermal ion dilution, electrostatic stabilization of micro-instabilities by the resonant interaction of fast particles with waves, and electromagnetic stabilization). Based on their results reported in reference,<sup>17</sup> these authors conjectured that zonal flows force-driven by Alfvén instabilities may be used to reduce the level of ITG turbulence.<sup>17</sup> This conjecture proposes a mechanism where forced-driven zonal flows mediate the indirect interaction between energetic particles and turbulence since a fraction of the energetic particles introduced in a reactor via auxiliary heating in a turbulent plasma can resonantly excite an Alfvén mode. Due to the contribution of these resonant energetic particles in the early nonlinear phase of the Alfvén mode dynamics (i.e., mostly via the curvature coupling term), the Alfvén modes can thus excite zonal flows via a force-driven process.<sup>16</sup> These excited zonal flows may, in turn, act on the background turbulence and mitigate it, as the simulations presented in Ref. 17 suggested. The statement of this conjecture is illustrated in Fig. 2.

At this point, it must be pointed out that the part of this conjecture was already “proven” by numerical simulations of reference,<sup>17</sup> which we have here recalled in Fig. 1, i.e., the part that predicts the

excitation of Alfvén modes by energetic particles in a turbulent plasma and the subsequent excitation of forced-driven zonal flows due to wave-wave interaction of these Alfvén modes. Instead, the other part of the conjecture that claims that forced-driven zonal flows can mitigate the background turbulence has never been tested due to the complexity of the self-consistent problem mentioned above.

### C. Contribution and outline of this study

In this work, we embark on a novel approach, designing numerical experiments to test the part of the above conjecture of Fig. 2, which claims that forced-driven zonal flows excited by Alfvén modes can be used to mitigate background turbulence. As mentioned before this is an inherently nonlinear complex problem. However, the causal connection we are looking for namely, the fact that zonal flows excited by Alfvén modes may concur to the mitigation of background turbulence induced by ITG modes can be studied in a simplified framework if we focus only on the effects of forced-driven zonal flows on the dynamics of the ITG instabilities (we recall indeed that the ITG instability occurs in the early phase of the simulation and saturates due to nonlinear processes to generate turbulence). In this sense, significant mitigation of the ITG instabilities by the forced-driven zonal flows would strongly indicate the stabilizing effect of forced-driven zonal flows on turbulence. This reformulation of the problem is based on the hypothesis that a strong mitigation of the instability will translate into a mitigation of the resulting turbulence, as quasi-linear approximations predict that a strong relationship exists between the anomalous diffusion coefficient and the linear growth rate of the instability.<sup>56,57</sup> Our objectives are twofold: to numerically study the dynamics of forced-driven zonal flows in the experimentally relevant scenario, to report the expected amplitude and saturation level of zonal flows forced-driven by an Alfvén mode excited by energetic particles, and to study the impact of such zonal flows on one of the most common drift wave instabilities (ITG), which is a major source of anomalous transport in tokamaks.

Aiming to resolve the problem of isolating the stabilization mechanism, which has been conjectured above from the other ITG stabilization mechanisms proposed in the literature, we have here performed two kinds of simulations. The first simulation aims to characterize the forced driven-zonal flows (i.e., measuring their amplitude radial structure and frequency) driven by Alfvén mode due to their resonant interactions with energetic particles. A second simulation is then performed using the zonal flows forced-driven by the Alfvén mode as a source to study the impact of the latter on ITG instability. We show that imposing this self-consistent forced-driven zonal flow obtained from the first simulation significantly mitigates the ITG instability, leading to a significant drop in its growth rate. The results we have obtained which we will discuss below, show that the forced-driven zonal flow stabilizes the ITG instability by scattering the mode from its unstable long-wavelength domain to its more stable short-wavelength domain. A zonal flow amplitude scan reveals the existence of an inverse relation between the zonal flow amplitude and the ITG growth rate.

This work is structured into four sections. Section I provides an introduction, explaining the motivations for this work. In Sec. II, we describe the ORB5 numerical scheme. Section III presents the dynamics of Alfvén modes and their nonlinear excitation of zonal flows. Finally, Sec. IV studies the dynamics of ITG and forced-driven zonal flows.

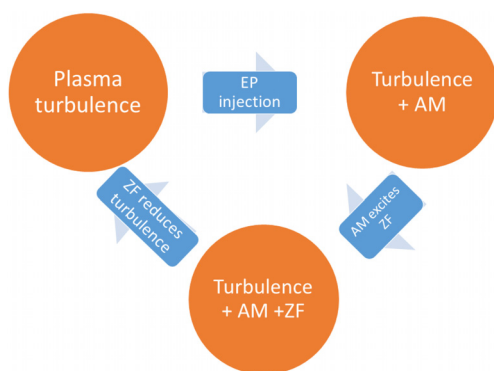


FIG. 2. Cartoon summarizing the conjecture we aim to verify with the numerical simulations discussed herein.



## II. MODEL

The main numerical tool used for the investigations described herein is the global electromagnetic particle-in-cell code ORB5.<sup>52,58</sup> ORB5 solves a full-f gyrokinetic Vlasov equation using a control variates scheme and perturbed field equations, i.e., quasineutrality of the background is assumed, and furthermore, the polarization density is linearized. The model equations of ORB5 derived using the mixed-variable gyro kinetic formalism are the gyro center trajectories [Eqs. (1) and (2)], quasi-neutrality equation [Eq. (4)], Ampère's equations [Eq. (5)], and the Ohm's law (Eq. (6)).

$$\frac{d\mathbf{R}}{dt} = v_{\parallel} \mathbf{b}_0^* + \frac{1}{eB_{\parallel}^*} \mathbf{b} \times \mu \nabla B + \frac{\mathbf{b}}{B_{\parallel}^*} \times \nabla \langle \phi - v_{\parallel} A_{\parallel}^{(s)} - v_{\parallel} A_{\parallel}^{(h)} \rangle - \frac{e}{m} \langle A_{\parallel}^{(h)} \rangle \mathbf{b}_0^*, \quad (1)$$

$$\frac{dv_{\parallel}}{dt} = -\frac{\mu}{m} \mathbf{b}_0^* \cdot \nabla B - \frac{e}{m} \left[ \mathbf{b}^* \cdot \nabla \langle \phi - v_{\parallel} A_{\parallel}^{(h)} \rangle + \frac{\partial}{\partial t} \langle A_{\parallel}^{(s)} \rangle \right] - \frac{\mu}{m} \frac{\mathbf{b} \times \nabla B}{B_{\parallel}^*} \cdot \nabla \langle A_{\parallel}^{(s)} \rangle, \quad (2)$$

$$\mathbf{b}^* = \mathbf{b}_0^* + \frac{\nabla \langle A_{\parallel}^{(s)} \rangle \times \mathbf{b}}{B_{\parallel}^*}, \quad \mathbf{b}_0^* = \mathbf{b} + \frac{mv_{\parallel}}{eB_{\parallel}^*} \nabla \times \mathbf{b}, \quad (3)$$

$$B_{\parallel}^* = B + \frac{mv_{\parallel}}{e} \mathbf{b} \cdot \nabla \times \mathbf{b}, \quad -\nabla \cdot \left( \frac{n_0}{B\Omega_i} \nabla_{\perp} \phi \right) = \bar{n}_i - \bar{n}_e, \quad (4)$$

$$\sum_{s=i,e} \frac{\beta_s}{\rho_s^2} A_{\parallel}^{(h)} + \nabla_{\perp}^2 A_{\parallel}^h = \mu_0 \sum_{s=i,e} \bar{J}_s + \nabla_{\perp}^2 A_{\parallel}^s, \quad (5)$$

$$\frac{\partial}{\partial t} A_{\parallel}^{(s)} + \mathbf{b} \cdot \nabla \phi = 0. \quad (6)$$

The long wavelength version of the quasi-neutrality equation is used for all simulations. The phase-space coordinates are  $\mathbf{Z} = (\mathbf{R}, v_{\parallel}, \mu)$ , i.e., respectively, the gyro center position, the parallel velocity, and the magnetic moment. The time-dependent fields are the scalar potential,  $\phi$ , and the parallel component of the vector potential, which is split into a symplectic and Hamiltonian part,  $A_{\parallel} = A_{\parallel}^{(s)} + A_{\parallel}^{(h)}$ .  $\mathbf{B}$  and  $\mathbf{b}$  are the equilibrium magnetic field and magnetic unit vector.  $\bar{n}_s$  and  $\bar{J}_s$  are the perturbed density and current, while  $\Omega_i$  is the ion cyclotron frequency. The other quantities are written in standard notation. The gyro average operator is defined by

$$\langle \phi \rangle = \frac{1}{2\pi} \int_0^{2\pi} \phi(\mathbf{R} + \boldsymbol{\rho}_L) d\alpha, \quad (7)$$

where  $\alpha$  here is the gyro angle and  $\rho_L = \rho_L(\alpha, \mu)$  is the Larmor radius. The gyro average operator reduces to the zeroth Bessel function  $J_0(k_{\perp} \rho_{L,i})$  if we transform it in Fourier space. The gyro average is calculated for all ion species (the same form applies to both fast and bulk ions). We consider the finite Larmor radius of ions, neglecting them for electrons. Hereafter, we will label with "s" the radial coordinate, which is defined in terms of poloidal flux,  $\psi_p$  as  $s = \sqrt{\psi_p / \psi_{p,edge}}$ . A nonlinear pullback scheme is used in all electromagnetic simulations. This scheme includes the nonlinear flutter terms, whose contribution becomes non-negligible for strongly unstable MHD-type modes.<sup>59</sup>

## III. ALFVÉN MODES DYNAMICS IN JET 92416

The first challenge in this section is to be able to run a global electromagnetic simulation with experimentally measured magnetic equilibrium, species temperature, and density profiles, in which Alfvén modes excited by energetic particles drive zonal flows. A good experimental case we will consider is the JET shot 92416 afterglow experiment.<sup>60,61</sup> In this shot,  $n = 4, 5, 6$  TAEs (Toroidal Alfvén eigenmodes) were measured at the time 6.2 s of the discharge. We shall consider the magnetic equilibrium and profiles at this particular time. This study focuses only on the dynamics of the  $n = 5$  mode. A successful benchmark of this mode has been performed without fast particles using the MISHKA code<sup>62</sup> and ORB5.

### A. JET 92416 equilibrium

JET is a tokamak with a minor radius,  $a_0 = 0.95$  m, major radius  $R_0 = 2.88$  m, and an on-axis magnetic field of  $B_0 = 3.4$  T. The safety factor on the axis and at the edge are  $q_0 = 1.74$  and  $q_{edge} = 4.6$ , respectively. The magnetic equilibrium and safety factor profile are generated from experimental data by the CHEASE code<sup>63</sup> (Fig. 3). The TRANSP code generated the thermal electrons, energetic species equilibrium profiles, and ion density<sup>64</sup> from experimental data (Fig. 4). However, this study considers a scenario where the electron and main ion species have the same temperature profile. A reference radial position  $s_0 = 0.0$ , is chosen from which the following physical quantities are calculated.  $\rho^* = \rho_s / a_0 = 3.08 \times 10^{-3}$  (with  $\rho_s$  the sound Larmor radius), the Alfvén speed,  $V_a = 7.56 \times 10^6$  m/s, the sound speed,  $c_s = 4.8 \times 10^5$  m/s, the cyclotron frequency,  $\Omega_i = 1.6 \times 10^8$  rad/s, and the thermal plasma beta,  $\beta = 0.9\%$ .

Global linear and nonlinear electromagnetic simulations were performed. The number of grid points for the radial, straight field line poloidal angle, and toroidal angle are  $(n_s, n_{\chi}, n_{\phi}) = (768, 192, 48)$ , respectively, a time step of  $dt = 3\Omega_i^{-1}$  and the number of markers for the thermal ions (Deuterium), electrons, and fast particles (Deuterium) are  $(N_i, N_e, N_f) = (32, 128, 32) \times 10^6$ , respectively. Fast particles in this shot were mostly generated by neutral beam injection (NBI). In this simulation, we model these fast particles using an equivalent Maxwellian, with an equivalent temperature calculated from the parallel and perpendicular NBI beam energy. No collisions are considered, unicity boundary conditions (the value of the scalar potential is fixed on the magnetic axis<sup>52</sup>) are imposed on the field. Drift kinetic heavy electrons are used to speed up the simulations ( $m_e/m_i = 0.005$ ). The radial domain for this simulation is  $[0, 1.0]$ , and a filter is used such that only the  $n = 0, 5$  toroidal modes are retained. The energetic particle dilution, which is the ratio of the volume-averaged energetic particle density to volume-averaged electron density for these simulations, is set to 10%, with the  $T_f/T_e = 25$  at the reference location,  $s_0$ . A convergence test showing the validity of these simulation parameters can be found in the Appendix, whose results are shown in Fig. 13.

### B. Linear Alfvén mode dynamics

At  $n = 5$ , Alfvén mode is excited by energetic particles in the linear phase of the simulation. Figure 5(a) plots the scalar potential associated with this mode in the poloidal plane. The color map on this plot represents the value of the scalar potential. The mode structure in this plane shows a clear, strong destabilization in the low field side of the

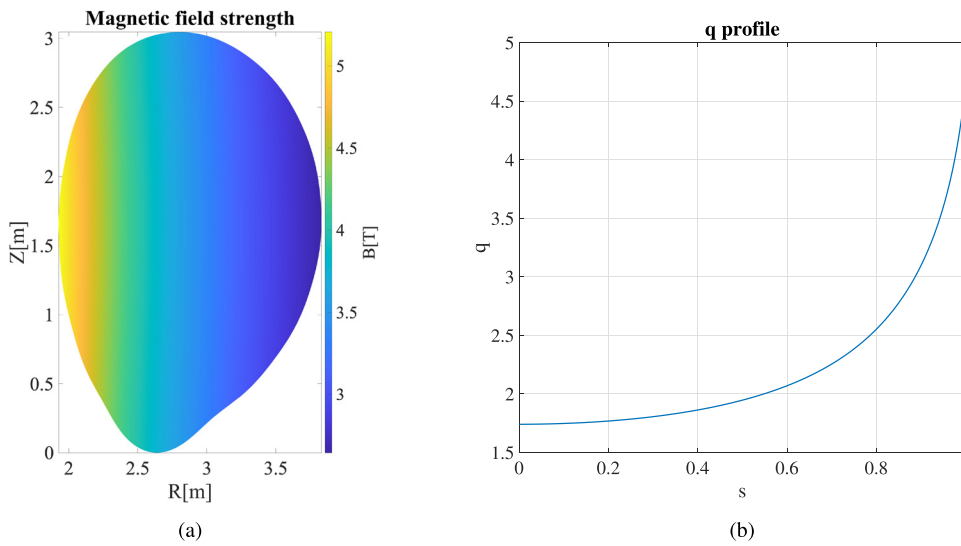


**FIG. 3.** Magnetic equilibrium and radial profile deduced from experimental data using the CHEASE code. (a) 2D plot of the magnetic field strength in the poloidal plane. (b) Safety factor  $q$  as a function of the normalized radial position  $s$ .

simulation domain, and the scalar potential has its maximum amplitude near the mid-radius. Thus, the excited mode has a ballooning structure. A deeper understanding of the structure of the excited Alfvén mode can be obtained by decomposing the mode's scalar potential into its constituent poloidal harmonics. Figure 5(b) plots the radial structure of the individual poloidal harmonics. This plot clearly shows the radial domain covered by the instability,  $[0.2, 0.8]$ , and the largest poloidal harmonic,  $m = 10$ . Two other poloidal harmonics with non-negligible amplitude exist  $m = 9, 11$ . In the low-shear large-aspect ratio limit, the eigenmode amplitude is not strongly localized around half-rational surfaces, and individual poloidal harmonics are active across an extended radial region as a result, these poloidal harmonics overlap. These poloidal harmonics are all excited by a single eigenmode, as can be confirmed by examining the temporal Fourier transform of the mode amplitude across the radial coordinate and comparing it to the radial structure of the poloidal harmonics in Fig. 6(a). The large amplitude at  $s = 0.5$  results from the coupling between the  $m = (9, 10)$  poloidal harmonics, while that at  $s = 0.62$  is due to the coupling between the  $m = (10, 11)$  poloidal harmonics. Despite significant amplitude elsewhere, the TAE amplitude peaks, as expected, at half rational surfaces  $q = (m + 1/2)/n$ , with harmonics  $m$  and  $(m + 1)$  most active at these positions.<sup>65</sup>

The excited mode resulting from the coupling between different poloidal harmonics at various radial locations has a growth rate and frequency,  $\gamma = 0.4935c_s/a$ , with a frequency of  $\omega \approx 0.24\omega_A$  ( $\sim 100$  kHz). This frequency falls in the TAE range (between 60 and 200 kHz). We can check that the excited modes are TAEs by comparing their radial localization and frequencies to the shear Alfvén continuum spectrum (SAW) corresponding to the equilibrium in question. The FALCON code<sup>66</sup> was used to calculate the SAW spectrum, and its result is overplotted on the power spectral density of simulation electric field vs frequency and radius obtained from ORB5 simulation, Fig. 6(b). We observe from this plot that the frequency of the excited mode is near the TAE gap. So, the excited Alfvén modes, are identified as TAEs. It should be noted that due to the high fraction of energetic particles used in this simulation, these particles are starting to have an effect on mode dispersion. This explains why the mode touches the continuum.

### C. Nonlinear Alfvén dynamics

A filter is applied in the nonlinear simulation to retain only the  $n = 0, 5$  toroidal modes. The simulation parameters described in Sec. III A are used. Figure 7, shows the time evolution of different poloidal harmonics. We can identify three phases from this plot: the linear growth phase from  $[0, 5000]\Omega_i^{-1}$ , the early saturation phase from  $[6000, 22000]\Omega_i^{-1}$  and the deep saturation phase  $[22000, 38000]\Omega_i^{-1}$ . The dynamics of the excited mode in each phase are different. The linear phase is characterized by wave-particle resonance interaction (wave-wave interactions are negligible) between the TAE and resonant energetic particles. Energy is transferred from resonant energetic particles to the TAE, causing it to grow at the rate reported in Sec. III B. The mode structure of the TAE changes negligibly in this phase as it grows in amplitude [Fig. 8(a)]. This phase is dominated by the  $m = 10$  harmonic, which has the highest amplitude. In the early nonlinear phase, wave-wave interaction becomes important. As the mode develops and drives  $n = 0$  modes, it, in turn, is modified due to nonlinear interactions, and a larger radial region and more poloidal harmonics become active. This coupling modifies the TAE mode structure, which was constant in the linear phase [Fig. 8(b)]. Part of the TAE energy is used to drive zonal flows, which is the  $n = 0$  toroidal mode (more details in Sec. III D). This nonlinear behavior eventually leads to the spreading of the instability to a wide radial domain,  $[0.1, 0.9]$  as shown in Fig. 8(c). The  $m = 9, 10, 11$  poloidal harmonics dominate the dynamics in this phase. In the deep nonlinear phase of the instability, the dominant poloidal harmonics of the early nonlinear phase have amplitudes that are of the same order of magnitude as the subdominant poloidal modes like the  $m = 8, 12$ , thereby leading to an even stronger and complex coupling between poloidal harmonics leading to a rapidly changing mode structure [Fig. 8(d)].

### D. Nonlinear excitation of zonal flows by TAEs

As discussed in Sec. III C, the TAE excites and drives zonal flows in the early nonlinear phase when wave-wave interactions become important. The excited TAE couples to the zonal flow ( $n = 0$ ) via wave-wave interactions and drives it in the early nonlinear phase,

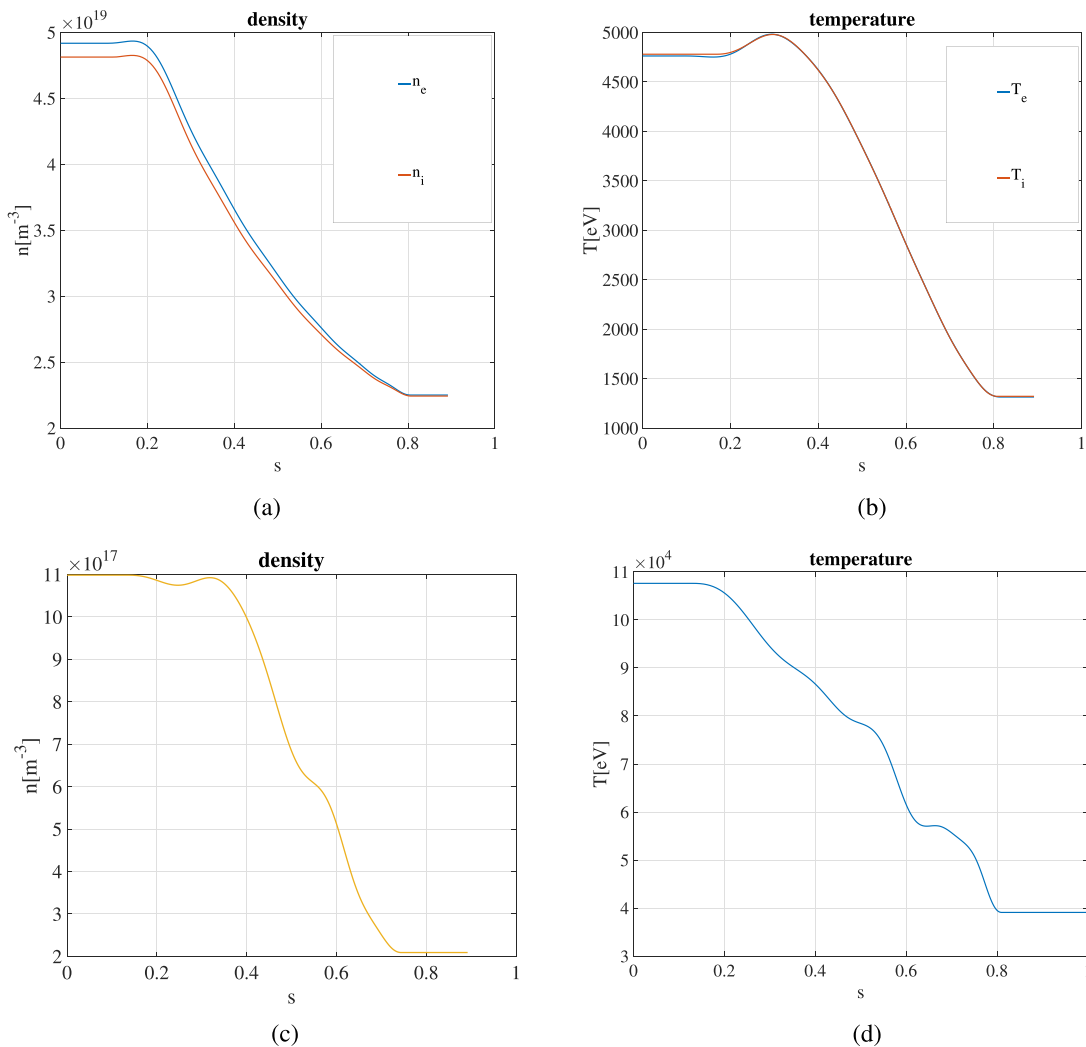


**FIG. 4.** Radial profiles deduced from experimental data thanks to the TRANSP code and taken as equilibrium initial conditions for the ORB5 simulation. (a) Density of thermal species, (b) temperature of thermal species, (c) density of energetic particles, and (d) temperature of energetic particles. Note  $s$  is the normalized radial coordinate.

which is still dominated by wave–particle interactions. The zonal flows are thus driven by a mechanism that does not require an amplitude threshold [Fig. 9(a)]. From theory, TAE has two possible mechanisms of zonal flow excitation: spontaneous excitation via modulational instability and force-driven excitation.<sup>16</sup> The spontaneous excitation of zonal flows via modulational instability by TAE is dominated by non-resonant bulk particle nonlinearity contribution to the Reynolds and Maxwell stresses. This process is dominant when wave–particle interaction is weak and requires that the amplitude of the driving mode be higher than a certain threshold. On the other hand, the force-driven excitation is dominated by resonant EP contribution in the linear growth stage of the pump TAE. In this case, the curvature-coupling-term due to the energetic particles response dominates over Reynolds and Maxwell stresses due to nonresonant thermal particles.<sup>16</sup> Zonal flows excited by this mechanism grow at a rate twice that of the TAE driving it. To distinguish the mechanism in play in our simulation, we

study the dynamics of the TAE and the zonal flows in the early nonlinear phase before saturation. In Fig. 9(a), the time evolution of the amplitudes of the TAE electric field and the zonal flow electric field is plotted. We can observe a rapid growth of the amplitude of the zonal flow in the interval  $[5000, 7000]\Omega_i^{-1}$ . Focusing on this time interval and measuring the growth rate of the zonal flow and the TAE, we find that the growth rate of the zonal flow is approximately twice that of the TAE, as shown in Fig. 9(b). This is evidence of force-driven excitation of zonal flows.<sup>16,50</sup> This zonal flow has a fine radial structure compared to the driving TAE radial envelope. The forced-driven zonal flow has a mesoscale radial envelope of the order of the width of the TAE radial envelope and a fine-scale structure. This fine-scale radial structure is visible in Figs. 9(c). This fine radial structure of zonal flows excited by Alfvén modes was also predicted in theory.<sup>16,67</sup> Hence, the resonant energetic particle response dominates the zonal flow driven by the TAE in this simulation. The TAE and the zonal flow saturate



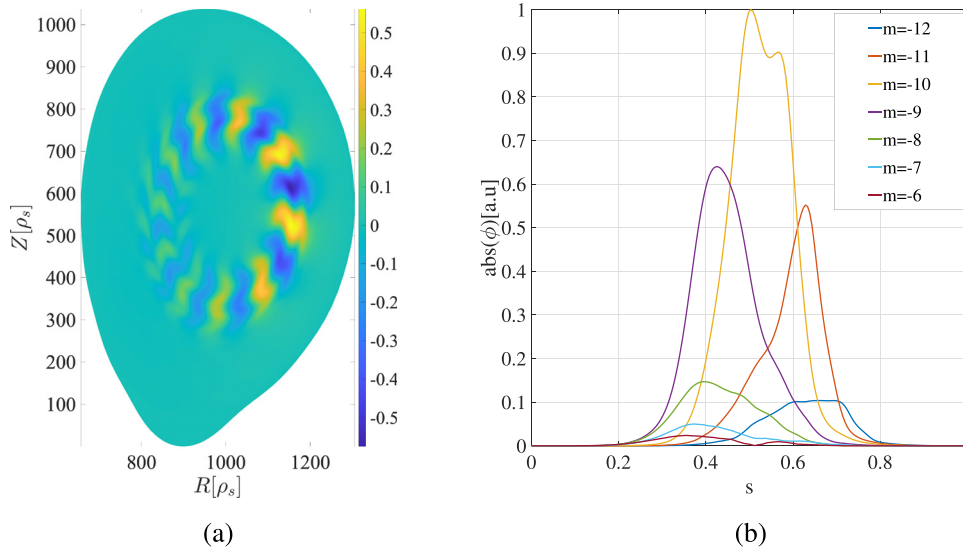


**FIG. 5.** Plots of the scalar potential from the linear Alfvén mode simulation. (a) Scalar potential plotted in the poloidal plane shows a strong mode destabilization in the low field side of the device, with the excited mode mostly localized close to the mid radius. (b) Radial mode structure of the scalar potential (in arbitrary units) of individual poloidal harmonics. The dominant poloidal harmonics ( $m = 9, 10, 11$ ) and the radial extent of the instability are visible. The excited mode has a frequency of about  $\omega \approx 0.24\omega_A$ . The parameters used for these simulations are described in Sec. III A. Note that  $s$  is the normalized radial coordinate and  $\rho_s$  is the sound Larmor radius.

with electric field amplitudes of 90 and 63.5 kV/m, respectively [Fig. 9(a)]. The amplitude of the zonal electric field is consistent with the magnitude of the same quantity measured in other JET shots, e.g., Fig. 7 in Ref. 68.

We characterize the forced-driven zonal flows after achieving this work’s first objective. A frequency analysis of this zonal flow shows that it is a zero-frequency zonal flow. The radial structure of the excited zonal flow and its associated shear is shown in Figs. 9(c) and 9(d). A final and very important property of the force-driven zonal flow is the shearing rate it generates. This shearing rate varies with radial position, as illustrated in Fig. 9(d), with an overall maximum shear of about  $\omega_{E \times B} \sim 0.4c_s/a$ . With these measurements, we can configure an

“antenna” in ORB5 to emulate this zonal flow in a simulation where we wish to measure its impact (see Sec. IV).

#### IV. EFFECTS OF FORCED-DRIVEN ZONAL FLOWS ON ITG DYNAMICS

We consider the same simulation parameters described in Sec. III A. However, electrons, in this case, are adiabatic, and we exclude energetic particles to avoid ITG mode stabilization due to thermal ion dilution. We only consider electrostatic fluctuations, as at low beta the ITG mode dynamics are not strongly dependent on beta.

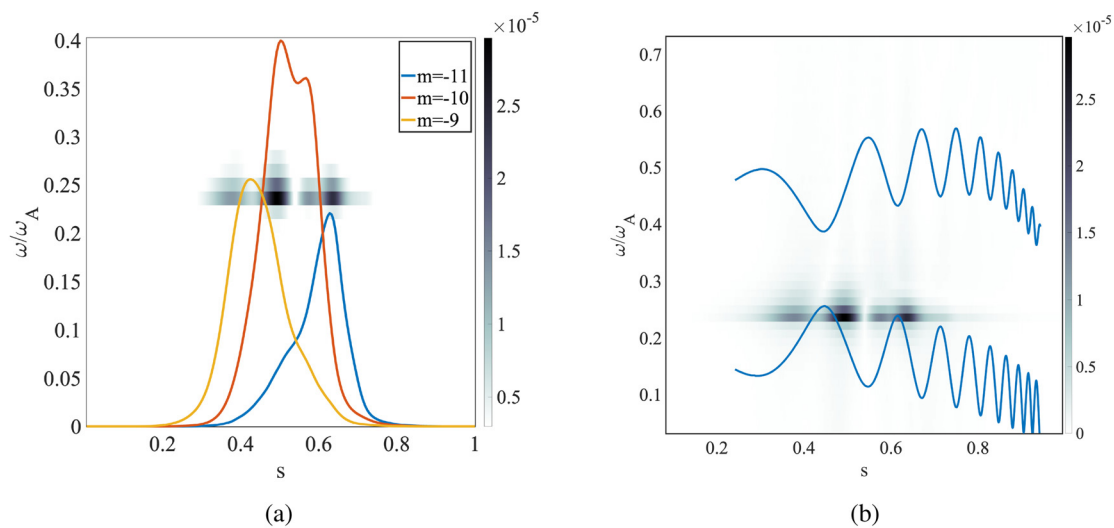


**FIG. 6.** The contour plot represents the fast Fourier transform in time of the electric field at every radial location obtained from ORB5 simulations minus the background growth rate vs frequency in units of the Alfvén frequency ( $\omega_A$ ) and radius ( $s$ ) from the linear Alfvén mode simulation. (a) With superimposed radial mode structure of the dominant poloidal harmonics of the scalar potential in arbitrary units (red, blue, and yellow curves). (b) With superimposed Alfvén continuum (blue curves) computed with the FALCON code. The parameters used for these simulations are described in Sec. III A.

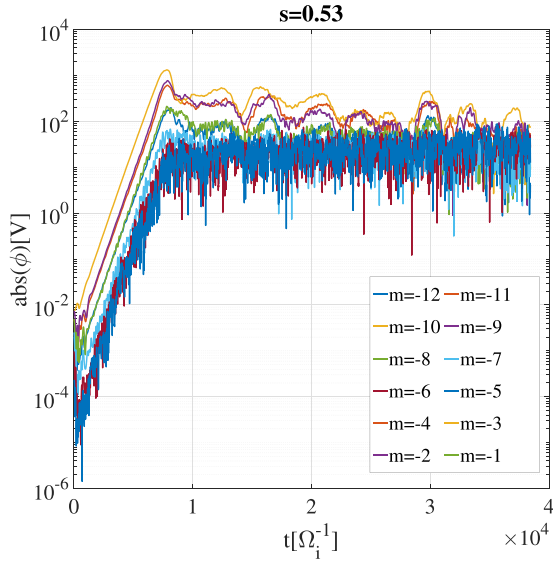


**FIG. 7.** Time evolution (with time in units of the inverse ion cyclotron frequency  $\Omega_i^{-1}$ ) of the absolute value of the amplitude of the scalar potential in volts (V) of individual poloidal harmonics of the excited TAE measured at  $s = 0.53$ , showing the instability's linear, early, and deep nonlinear phases in the nonlinear Alfvén mode simulation. The parameters used for these simulations are described in Sec. III A.

### A. Dynamics in the absence of zonal flows

To measure the effects of the forced-driven zonal flows on ITG instability in this experimental scenario, we first have to study the dynamics of this instability without any source of zonal flows. The instability in these simulations is driven by the strong temperature gradient in the thermal ion profile close to the mid-radius of the device. The ITG instability is strongest on the low-field side of the device, as shown in Figs. 10(a) and 10(b). A scan of toroidal mode numbers is performed, and the corresponding linear ITG growth rates are measured. Unstable ITG modes are measured for toroidal mode numbers in the range  $\{15,95\}$ . The fastest-growing ITG mode has a toroidal mode number of  $n = 70$  [see the mode structure in Fig. 10(b)] and a growth rate of  $\gamma \approx 0.14c_s/a$ , as shown in Fig. 10(c).

### B. The ORB5 antenna module

The antenna module, first implemented in ORB5 by Ohana and coworkers,<sup>69,70</sup> was designed to study the impact of specific plasma modes on the dynamics of plasma instabilities or turbulence. The antenna acts like an external source whose field can emulate a specific plasma mode given the frequency ( $\omega$ ), toroidal ( $n$ ), and poloidal ( $m$ ) mode numbers, the radial structure of the mode [ $h(s)$ ] and the phase offset ( $\Phi$ ). However, the antenna and plasma field are considered separately so that in linear simulations, only the plasma fields are linearized, keeping the antenna fields in the particle's characteristics. This configuration makes using the antenna for linear and nonlinear studies possible. In its simplest form, the antenna field,  $F_{ant}$ , can be written as

$$F_{ant} = h(s) \text{Re} \left[ \sum_{j=1}^N A_j e^{i(m_j \theta + n_j \varphi + \Phi_j)} (\alpha + \beta e^{i\omega t}) \right], \quad (8)$$

where  $A_j$  is the Fourier mode coefficient,  $\alpha$  and  $\beta$  are, respectively, the coefficients of the static and oscillating components. The quantity  $F_{ant}$  can be the electrostatic potential  $\phi$  and/or the parallel vector potential  $A_{||}$ . In this work, we used only the electrostatic antenna component. For this study, the zonal flows described in Sec. III D can be emulated by the ORB5 antenna module by setting  $m_j = n_j = \omega = \Phi_j = 0$ . In contrast, the scalar potentials corresponding to zonal electric field structures shown in Fig. 9(c) are loaded into  $h(s)$ . In the presence of the antenna, particle characteristics are modified as follows:

$$\begin{aligned} \frac{d\mathbf{R}}{dt} = & v_{||} \mathbf{b}_0^* + \frac{1}{eB_{||}^*} \mathbf{b} \times \mu \nabla B \\ & + \varepsilon_\delta \left[ \frac{\mathbf{b}}{B_{||}^*} \times \nabla \langle \phi - v_{||} A_{||}^{(s)} - v_{||} A_{||}^{(h)} \rangle - \frac{e}{m} \langle A_{||}^{(h)} \rangle \mathbf{b}_0^* \right] \\ & + \varepsilon_{ant} \left[ \frac{\mathbf{b}}{B_{||}^*} \times \nabla \langle \phi_{ant} - v_{||} A_{||ant}^{(s)} - v_{||} A_{||ant}^{(h)} \rangle - \frac{e}{m} \langle A_{||ant}^{(h)} \rangle \mathbf{b}_0^* \right], \end{aligned} \quad (9)$$

$$\begin{aligned} \frac{dv_{||}}{dt} = & -\frac{\mu}{m} \mathbf{b}_0^* \cdot \nabla B - \varepsilon_\delta \left( \frac{e}{m} \left[ \mathbf{b}^* \cdot \nabla \langle \phi - v_{||} A_{||}^{(h)} \rangle + \frac{\partial}{\partial t} \langle A_{||}^{(s)} \rangle \right] \right. \\ & \left. - \frac{\mu}{m} \frac{\mathbf{b} \times \nabla B}{B_{||}^*} \cdot \nabla \langle A_{||}^{(s)} \rangle \right) \\ & - \varepsilon_{ant} \left( \frac{e}{m} \left[ \mathbf{b}^* \cdot \nabla \langle \phi_{ant} - v_{||} A_{||ant}^{(h)} \rangle + \frac{\partial}{\partial t} \langle A_{||ant}^{(s)} \rangle \right] \right. \\ & \left. - \frac{\mu}{m} \frac{\mathbf{b} \times \nabla B}{B_{||}^*} \cdot \nabla \langle A_{||ant}^{(s)} \rangle \right), \end{aligned} \quad (10)$$

where  $A_{||ant}$  and  $\phi_{ant}$  are, respectively, the antenna's parallel component of the vector potential and the scalar potential, given in Eq. (8). The terms multiplied by  $\varepsilon_\delta$  are the self-consistent plasma fields, while those multiplied by  $\varepsilon_{ant}$  are the field emulated by the antenna. In a linear simulation, only the terms multiplied by  $\varepsilon_\delta$  are neglected. This way, the antenna can be used in linear simulations to study the impact of a specific mode on the linear dynamics of an instability. This approach is used in Sec. IV C study the effects of the forced-driven zonal flow characterized in Sec. III D on linear ITG dynamics.

### C. ITG dynamics in the presence of forced driven zonal flows

This section uses the ORB5 antenna module described earlier as a source of the zonal flows forced-driven by the  $n = 5$  TAE. The excited zonal flow is a ZFZF, with  $n = m = 0$ . The radial structure of the scalar potential from which the zonal electric field is derived is loaded into the antenna module. The temperature gradients in the ion profile still drive the ITG instability. However, the antenna module is switched on in all simulations, emulating the forced-driven zonal flows. We perform single toroidal mode ITG simulations and scan over the unstable toroidal mode number discussed in Sec. IV A. The ITG growth rates in the presence of the ORB5 antenna emulating the forced-driven zonal flow are measured. This zonal flow significantly mitigates the ITG instability, measured by the significant reduction of the growth rate of the most unstable mode that dominates the linear dynamics. All toroidal mode numbers are strongly stabilized in the presence of forced-driven zonal flows, and the range of unstable modes is correspondingly

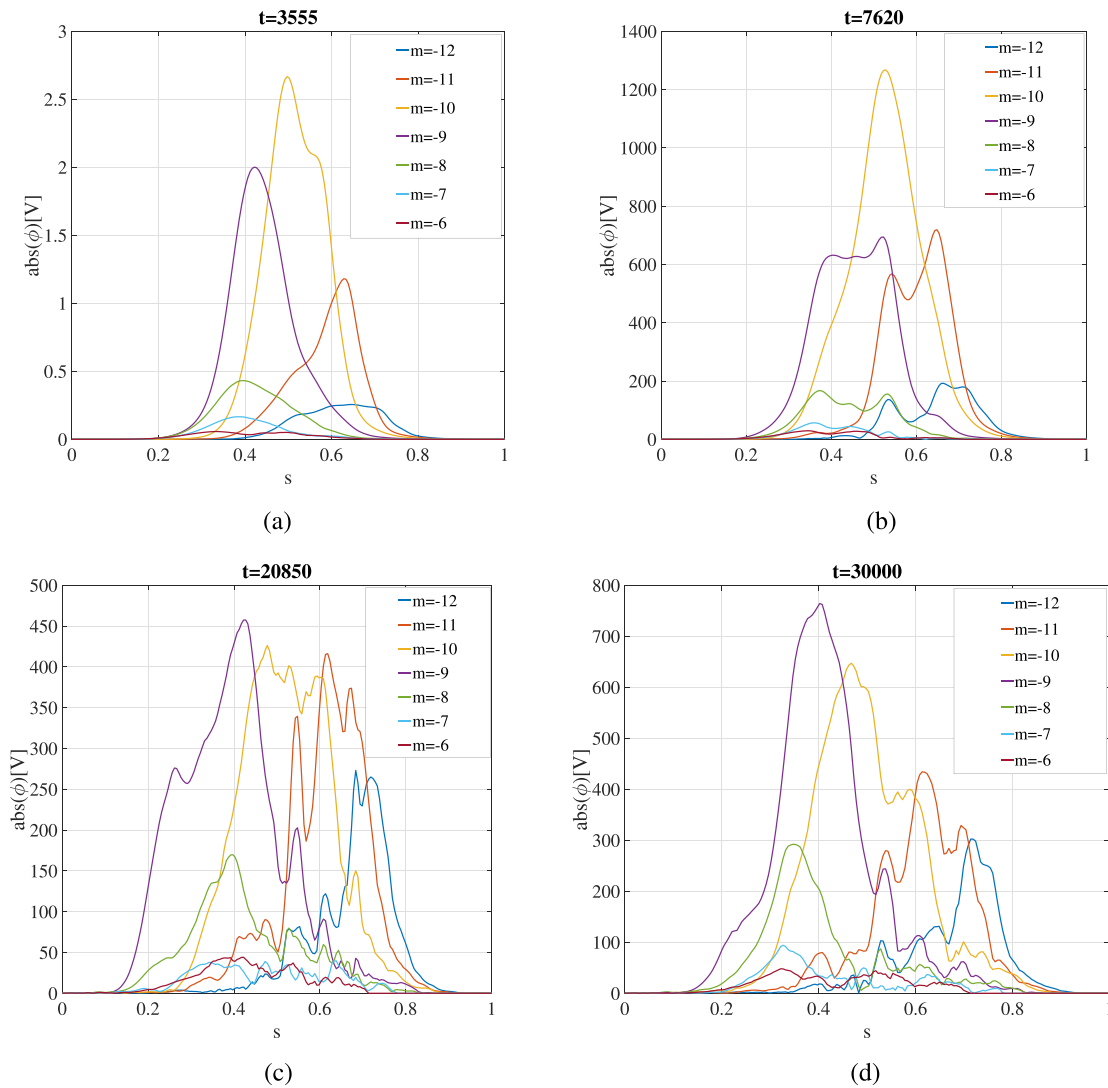


**FIG. 8.** Snapshots of the radial mode structure of the individual poloidal harmonics of the scalar potential showing how the TAE structure is modified in the nonlinear Alfvén mode simulations. The scalar potential is units of volts (V).  $s$  is the normalized radial coordinate. (a) Linear phase (b) Early nonlinear phase (before saturation). (c) Early nonlinear phase (after saturation). (d) Deep nonlinear phase. The parameters used for these simulations are described in Sec. III A.

reduced [Fig. 11(a)]. The forced-driven zonal flows stabilize the unstable ITG modes by scattering them from their unstable long-wavelength regime to their more stable short-wavelength regime.<sup>13</sup> The radial scattering of the unstable ITG mode can be observed in real space by following the evolution of the radial envelope of a single ITG mode before and after the zonal flow is activated in the simulation. Figure 12(a) shows the evolution of  $n = 70$  ITG radial envelope before and after switching the antenna module. Without the zonal flows, the radial envelope has a Gaussian shape (long-wavelength). However, when zonal flows are included in the simulations, the interaction between the forced-driven zonal flows and the unstable ITG modes results in a scattering of the unstable ITG mode. This scattering modifies its radial envelope, but the mode remains on its rational surface long after the antenna is switched on [see the amplitude after the

antenna is switched on in Fig. 12(a)]. However, the mode shifts from its reference rational surface toward the end of the simulations, and this might also be consistent with an  $E \times B$  shearing activity (the amplitude of the shearing rate is of the same order of magnitude as the growth rate of the fastest-growing mode). Looking at the same simulation in the Fourier space, Fig. 12(b), we observe that the scattering of the radial mode envelope in real space induced by the zonal flow corresponds to a shift in the radial wavenumber spectrum in Fourier space. The ITG radial wavenumber shifts from their low wavenumber domain, where they are unstable, to their more stable high wavenumber domain, consistently with Refs. 13 and 49. A similar mechanism occurs for all the unstable ITG modes, explaining the stabilization observed in Fig. 11(a). This result shows that mitigating ITG instability by forced-driven zonal flows is significant in experimentally relevant

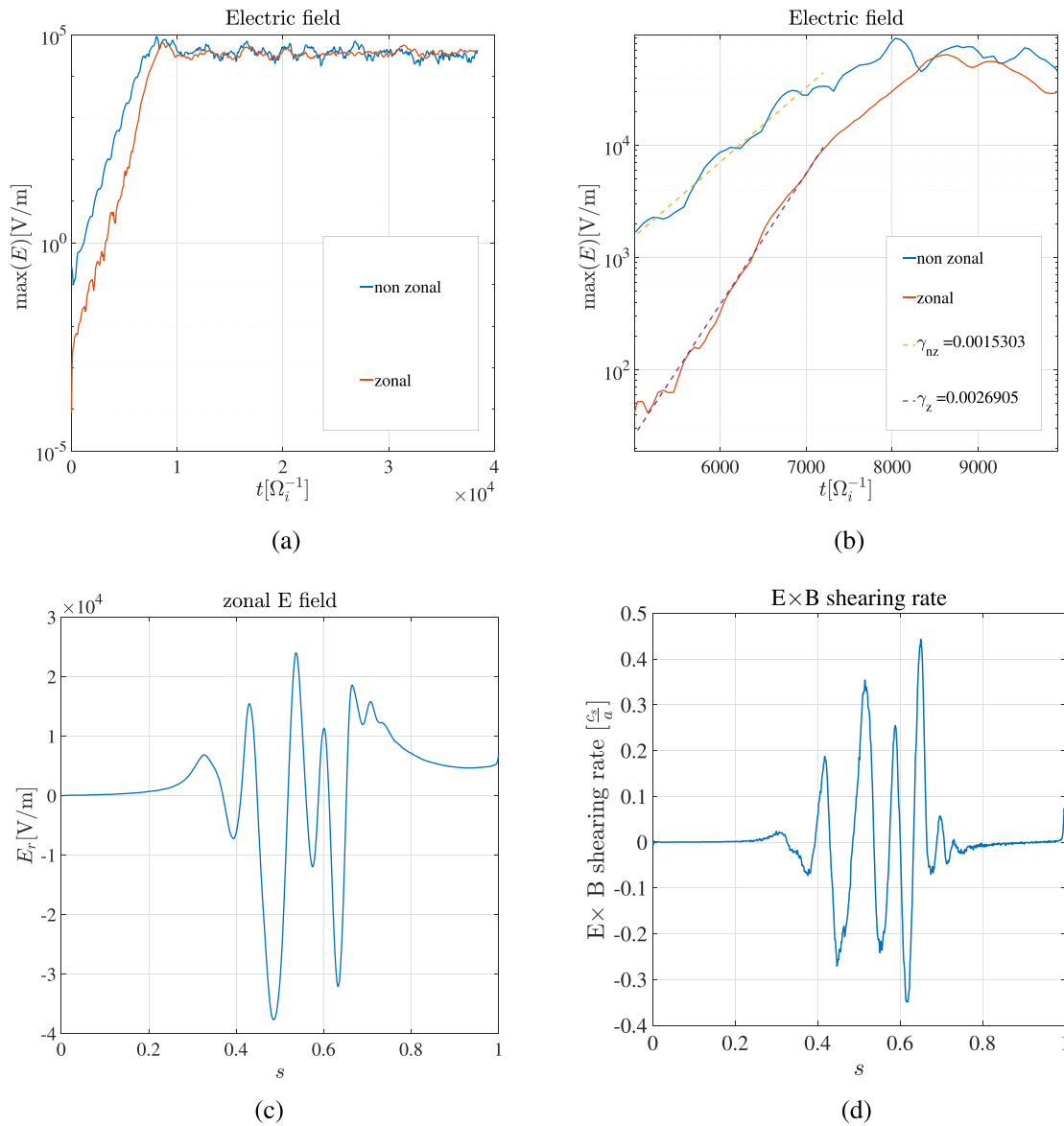


**FIG. 9.** Plots from the nonlinear Alfvén mode simulations. (a) Time evolution (with time in units of the inverse ion cyclotron frequency  $\Omega_i^{-1}$ ) of the absolute value of the amplitude electric field measured in volts per meter (V/m) decomposed into a zonal component (ZF) and nonzonal component (TAE) showing the excitation of ZF by TAE in the early nonlinear phase. (b) Zoom of early nonlinear phase showing ZF growing nearly two times faster than TAE. (c) Zonal flow radial structure in the saturation phase. The theoretically predicted fine radial structure of the ZF can be observed. (d) The zonal flow ExB shearing rate in units of the ion sound speed ( $c_s$ ) divided by the minor radius ( $a$ ) in the saturation phase. Note that  $s$  is the normalized radial coordinate.

conditions. Hence, these results show that forced-driven zonal flows can stabilize unstable ITG instability by scattering them from the domain of unstable low radial wavenumber radial domain to their more stable high wavenumber domain. This result confirms the claim that forced-driven zonal flows can mitigate ITG instability. This result is, however, not complete since we have tested only a quite specific scenario. We can expect significant energetic particle population and temperature differences in different experimental scenarios. These differences generally result in changes in the Alfvén modes and zonal

flow saturation levels. It is therefore important to study how the zonal flow amplitude affects the stabilization of ITG modes in order to generalize these results. To this end, we focus on the most unstable linear mode, i.e.,  $n = 70$ , and perform a zonal flow amplitude scan while keeping its radial structure constant. We can observe that amplitudes in the range  $[10^{-1}, 10^2]V$  produce little or no effect on the linear growth rate of the unstable ITG mode. This observation can be explained by the fact that, for this range of values, the interaction between the very low amplitude forced-driven zonal flow results in

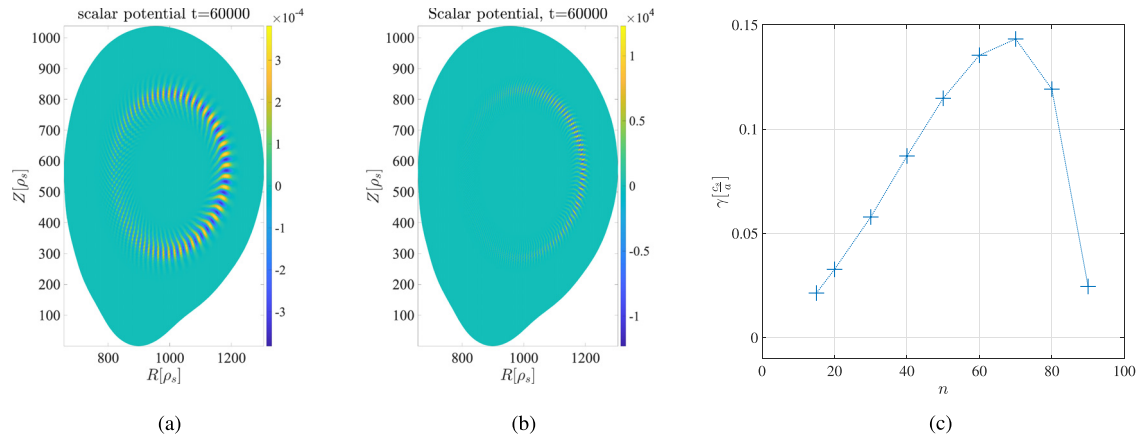


**FIG. 10.** Plots of the ITG 2D mode structure and growth rate from linear simulations without antenna. (a) Scalar potential plotted in the poloidal plane shows a strong  $n = 20$  ITG mode destabilization in the low field side of the device, with the excited mode mostly localized close to the mid radius where the ion temperature has the strongest gradient. (b) Scalar potential plotted in the poloidal plane shows a strong  $n = 70$  ITG mode destabilization in the low field side of the device, with the excited mode mostly localized close to the mid radius where the ion temperature has the strongest gradient. (c) A plot of the linear ITG growth rate ( $\gamma$ ) in units of the ion sound speed ( $c_s$ ) divided by the minor radius (a) vs the toroidal mode number.

scattering that does not significantly modify the mode structure. Hence, the radial wavenumber does not change significantly. Beyond this amplitude range, increasing the zonal flow amplitude leads to a stronger scattering of the drift wave due to a stronger interaction between the ITG and the zonal flow, pushing the ITG radial mode structure to significantly larger radial wave numbers, leading to stabilization, as depicted in Fig. 11(b). This inverse relation between the zonal flow amplitude and the ITG instability growth rate has also been reported in the literature.<sup>41,71</sup> This scan reveals that for efficient stabilization of ITG by forced-driven zonal flows, the zonal flows must be driven to high amplitude for optimal stabilization by scattering. The increase in zonal flow amplitude, even by keeping the zonal flow radial

structure constant, translates into a stabilization of the ITG. This is consistent with the theoretical predictions.<sup>13,49</sup>

To conclude, the significant mitigation of the ITG instabilities by the forced-driven zonal flows we have demonstrated in this study suggests that the forced-driven zonal flows reported by Biancalani *et al.* in Ref. 17 play a non-negligible role in the mitigation of the ITG turbulence reported therein. The linear results presented in this article can be used to interpret the nonlinear interaction between forced-driven zonal flows and turbulence since quasi-linear theory predicts a strong relationship between anomalous diffusion coefficient and the linear growth rate of the instability.<sup>56,57</sup> Hence, a significant modification in the linear physics of instability could also translate into the resulting

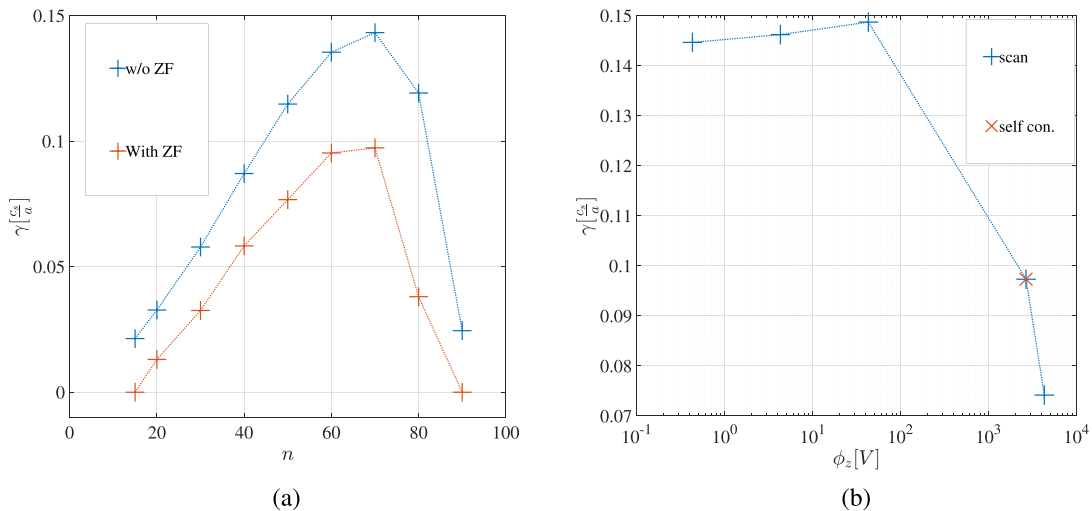


**FIG. 11.** Plot of the ITG growth rate in units of the ion sound speed ( $c_s$ ) divided by the minor radius vs toroidal mode number and zonal flow amplitude in volts (V) for the linear ITG simulations with antenna emulating forced-driven zonal flows. (a) ITG growth rate vs toroidal mode number with and without forced-driven zonal flows, for the parameters and equilibrium configuration discussed in Sec. III A. (b) Zonal flow amplitude scan, showing stronger stabilization for higher amplitudes.



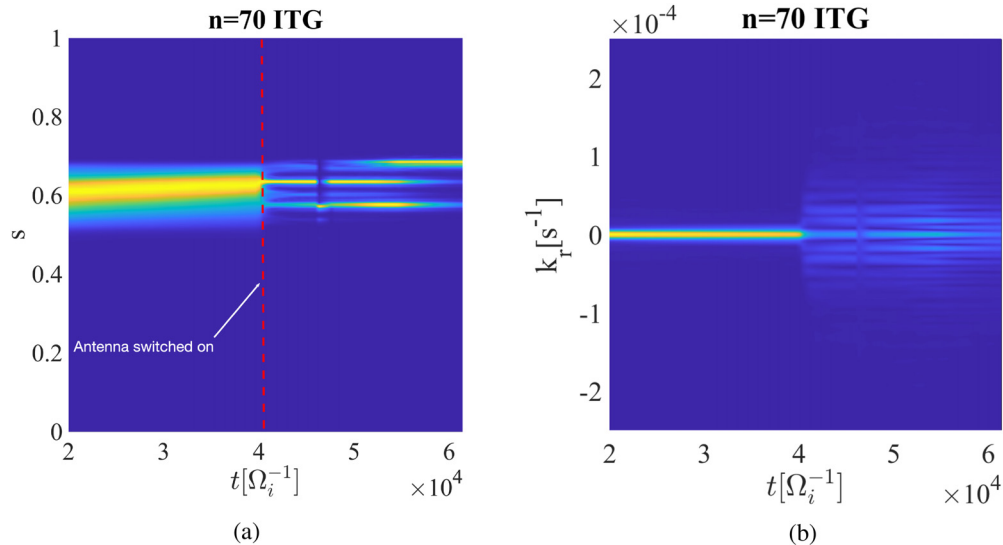


**FIG. 12.** (a) Plot of the time evolution of the radial envelope of the scalar potential vs radial position of the  $n = 70$  ITG showing a scattering of its radial envelope due to interaction with the zonal flow. The red line indicates when the “antenna” is switched on. (b) The plot of the time evolution of the absolute value of the Fourier transform of the scalar potential in radial position vs radial wave number. This plot shows the scattering of the mode in Fourier space from lower wavenumbers to higher wavenumbers.

nonlinear physics (turbulence transport). The conjecture proposed in Ref. 17 does not take into account the strong heat fluxes that can be induced by the Alfvén modes due to their excitation by energetic particles, which is in turn reported in reference.<sup>72</sup> More research is ongoing in this direction, studying the regimes and parameters in which the forced-driven zonal flows can significantly mitigate background turbulence with Alfvén modes driving significantly lower fluxes, resulting in better confinement overall. This interesting scenario has been observed in the JET shots reported in the references.<sup>37,38</sup> Data from these shots show improved thermal confinement even in the presence of various Alfvén modes.

## V. CONCLUSION

In this work, we investigated a possible indirect interaction mechanism of energetic particles and turbulence mediated by forced-driven zonal flows. This mechanism was proposed in reference.<sup>17</sup> It is grounded on the idea that forced-driven zonal flows excited by the linearly unstable Alfvén modes can mitigate background turbulence generated by ITG instabilities. In order to test this conjecture, we designed some “*ad hoc*” numerical experiments in the first nonlinear simulation, where we studied the dynamics of zonal flows forced-driven by Alfvén modes excited by energetic particles in a self-consistent, gyrokinetic description accounting for electromagnetic fluctuations. These excited zonal flows were measured, and their parameters were used to configure the antenna module of ORB5, which was used to emulate (the antenna plays the role of a source of forced-driven zonal flows) the zonal flows. A second set of electrostatic linear ITG simulations was thus made with the configured antenna emulating the forced-driven zonal flows to study the effect of the Alfvén mode-driven zonal flows on the ITG dynamics. Setting the experiment in this way permitted us to focus only on the effects of the forced-driven zonal flows. The study used magnetic equilibrium and species profiles generated from experimental data from the JET shot 92416 Afterglow experiment.

In the Alfvén mode simulations, we found that the excited  $n = 5$  mode was a TAE as its frequency falls in the TAE gap of the continuum spectrum corresponding to this equilibrium. This TAE nonlinearly excited a zero frequency zonal flow with fine radial structure and a growth rate that was twice that of the TAE, evidence of forced-driven excitation.<sup>16</sup> The quantitative features of the excited zonal flow have been identified, and its parameters were used to configure an antenna in ORB5, which acts as a source of forced-driven zonal flows. Running linear ITG simulation with the ORB5 antenna emulating the forced-driven zonal flows, we found that ITG dynamics were significantly affected, leading to a significant reduction in the growth rate of these modes. The forced-driven zonal flows stabilized the linearly unstable ITG by scattering them into their short wavelength stable domain. This is proven by comparing the radial structure of the ITG modes, respectively obtained in the absence and presence of the ZF. In the presence of the ZF, the ITG mode radial structure is dominated by a higher radial wavenumber. These results show that in experimentally relevant conditions, the zonal flows, forced-driven by Alfvén modes due to their excitation by energetic particles, can significantly impact the ITG instability dynamics once the amplitude of the forced-driven is large enough to scatter the unstable ITG to larger radial wavenumber more stable domain. This results in an inverse relation between the zonal flow amplitude and the instability growth rate.

The study we have conducted shows that forced-driven zonal flows significantly reduce ITG instabilities. This demonstrates that these flows play a non-negligible role in mitigating ITG turbulence, as first suggested in reference.<sup>17</sup> The linear results in this article can help us understand the nonlinear interaction between forced-driven zonal flows and turbulence. Quasi-linear theory suggests a strong connection between the anomalous diffusion coefficient and the linear growth rate of the instability. Hence, the significant modification in the linear physics of the instability should also translate into the resulting nonlinear physics (turbulence). We, however, recall here that the conjecture

proposed in reference,<sup>17</sup> does not take into account the strong heat fluxes that can be induced by the Alfvén modes due to their excitation by energetic particles, which is reported in reference.<sup>72</sup> More research is currently being conducted in this field, analyzing the conditions and regimes under which the forced-driven zonal flows can effectively reduce background turbulence with Alfvén modes, leading to significantly lower fluxes, and thus, better overall confinement.

## ACKNOWLEDGMENTS

This work was partially supported by the “Lorraine Université d’Excellence” Doctorate funding (project R01PKJUX-PHD21) belonging to the Initiative “I-SITE LUE.” Part of this work has been carried out within the framework of the EUROfusion Consortium, funded by the European Union via the Euratom Research and Training Programme (Grant Agreement No.101052200 EUROfusion). Views and opinions expressed here are, however, those of the authors only and do not necessarily reflect those of the European Union or the European Commission. Neither the European Union nor the European Commission can be held responsible for them. Numerical calculations for this work have been partially performed on the cluster Explor of the “Maison de la simulation Lorraine” (We are grateful to the partial time allocation under project No. 2019M4XXX0978) and on the MARCONI FUSION HPC system at CINECA. Discussions with Ivan Novikau about the antenna module of the gyrokinetic code ORB5 are gratefully acknowledged. The authors are grateful to Etienne Gravier and Maxime Lesur (IJL, Nancy), to Fulvio Zonca (CNPS, Frascati, Italy), and Zhixin Lu (IPP, Garching, Germany) for valuable discussions and remarks.

## AUTHOR DECLARATIONS

### Conflict of Interest

The authors have no conflicts to disclose.

### Author Contributions

**J. N. Sama:** Conceptualization (equal); Data curation (equal); Formal analysis (equal); Investigation (equal); Methodology (equal); Resources (equal); Software (equal); Validation (equal); Visualization (equal); Writing – original draft (lead); Writing – review & editing (equal). **A. Biancalani:** Conceptualization (equal); Formal analysis (equal); Funding acquisition (equal); Methodology (equal); Project administration (equal); Resources (equal); Software (equal); Supervision (equal); Validation (equal); Writing – review & editing (equal). **A. Bottino:** Formal analysis (equal); Methodology (equal); Software (equal); Supervision (equal); Validation (equal); Writing – review & editing (equal). **D. Del Sarto:** Conceptualization (equal); Formal analysis (equal); Funding acquisition (equal); Methodology (equal); Resources (equal); Software (equal); Supervision (equal); Validation (equal); Writing – review & editing (equal). **R. J. Dumont:** Resources (equal); Validation (equal); Writing – review & editing (equal). **G. Di Giannatale:** Validation (equal); Writing – review & editing (equal). **A. Ghizzo:** Conceptualization (equal); Formal analysis (equal); Funding acquisition (equal); Investigation (equal); Methodology (equal); Resources (equal); Software (equal); Supervision (equal); Validation (equal); Writing – review & editing (equal). **T. Hayward-Schneider:** Formal analysis (equal); Investigation

(equal); Methodology (equal); Resources (equal); Software (equal); Supervision (equal); Validation (equal); Visualization (equal); Writing – review & editing (equal). **Ph. Lauber:** Conceptualization (equal); Formal analysis (equal); Investigation (equal); Methodology (equal); Supervision (equal); Validation (equal); Visualization (equal); Writing – review & editing (equal). **B. McMillan:** Formal analysis (equal); Investigation (equal); Validation (equal); Visualization (equal); Writing – review & editing (equal). **A. Mishchenko:** Formal analysis (equal); Methodology (equal); Resources (equal); Software (equal); Validation (equal); Visualization (equal); Writing – review & editing (equal). **M. Murugappan:** Validation (equal); Writing – review & editing (equal). **B. Rettino:** Validation (equal); Writing – review & editing (equal). **B. Rofman:** Validation (equal); Writing – review & editing (equal). **F. Vannini:** Validation (equal); Writing – review & editing (equal). **L. Villard:** Formal analysis (equal); Investigation (equal); Methodology (equal); Resources (equal); Software (equal); Validation (equal); Writing – review & editing (equal). **X. Wang:** Validation (equal); Writing – review & editing (equal).

## DATA AVAILABILITY

The data that support the findings of this study are available from the corresponding author upon reasonable request.

## APPENDIX: CONVERGENCE TEST OF NONLINEAR ALFVÉN MODE SIMULATION

We performed a convergence test on the simulation parameters on  $dr$  and  $dt$  which are the step heights of the radial and temporal grid, respectively. A convergence test on the number of markers

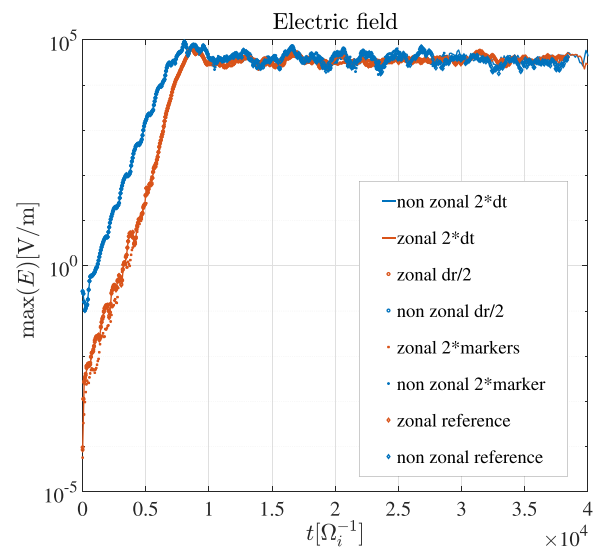


**FIG. 13.** Plots showing multiple simulations ran with ORB5 with different parameters for the time step  $dt$ , the radial step  $dr$ , and the number of numerical markers for the nonlinear Alfvén modes simulations with ORB5. The blue curves represent the amplitude of the electric field minus the fluxed surface averaged electric field in volts per meter (V/m). The red curves represent the amplitude of the flux surface average electric field in volts per meter (V/m). Time is in units of the ion cyclotron frequency  $\Omega_i^{-1}$ .

was also performed. The results of these simulations are summarized in Fig. 13. We observe that the simulations all converge for the parameter set tested.

## REFERENCES

- <sup>1</sup>A. Hasegawa, C. G. MacLennan, and Y. Kodama, "Nonlinear behavior and turbulence spectra of drift waves and Rossby waves," *Phys. Fluids* **22**, 2122–2129 (1979).
- <sup>2</sup>M. N. Rosenbluth and F. L. Hinton, "Poloidal flow driven by ion-temperature-gradient turbulence in tokamaks," *Phys. Rev. Lett.* **80**, 724–727 (1998).
- <sup>3</sup>F. Zonca, R. B. White, and L. Chen, "Nonlinear paradigm for drift wave–zonal flow interplay: Coherence, chaos, and turbulence," *Phys. Plasmas* **11**, 2488–2496 (2004).
- <sup>4</sup>N. Winsor, J. L. Johnson, and J. M. Dawson, "Geodesic acoustic waves in hydromagnetic systems," *Phys. Fluids* **11**, 2448–2450 (1968).
- <sup>5</sup>A. Biancalani, A. Bottino, C. Ehrlacher, V. Grandgirard, G. Merlo, I. Novikau, Z. Qiu, E. Sonnendrücker, X. Garbet, T. Görler, S. Leerink, F. Palermo, and D. Zarzoso, "Cross-code gyrokinetic verification and benchmark on the linear collisionless dynamics of the geodesic acoustic mode," *Phys. Plasmas* **24**, 062512 (2017).
- <sup>6</sup>I. Novikau, A. Biancalani, A. Bottino, G. D. Conway, U. D. Gürcan, P. Manz, P. Morel, E. Poli, and A. Di Siena, and A. U. Team, "Linear gyrokinetic investigation of the geodesic acoustic modes in realistic tokamak configurations," *Phys. Plasmas* **24**, 122117 (2017).
- <sup>7</sup>J. Sama, A. Biancalani, A. Bottino, I. Chavdarovski, D. Del Sarto, A. Ghizzo, T. Hayward-Schneider, P. Lauber, B. Rettino, F. Vannini *et al.*, "Effect of temperature anisotropy on the dynamics of geodesic acoustic modes," *J. Plasma Phys.* **89**, 905890109 (2023).
- <sup>8</sup>A. Ghizzo and F. Palermo, "Shear-flow trapped-ion-mode interaction revisited. I. Influence of low-frequency zonal flow on ion-temperature-gradient driven turbulence," *Phys. Plasmas* **22**, 082303 (2015).
- <sup>9</sup>A. Ghizzo and F. Palermo, "Shear-flow trapped-ion-mode interaction revisited. II. Intermittent transport associated with low-frequency zonal flow dynamics," *Phys. Plasmas* **22**, 082304 (2015).
- <sup>10</sup>T. Drouot, E. Gravier, T. Reveille, and M. Collard, "Self-generated zonal flows in the plasma turbulence driven by trapped-ion and trapped-electron instabilities," *Phys. Plasmas* **22**, 102309 (2015).
- <sup>11</sup>E. Gravier, M. Lesur, T. Reveille, T. Drouot, and J. Médina, "Transport hysteresis and zonal flow stimulation in magnetized plasmas," *Nucl. Fusion* **57**, 124001 (2017).
- <sup>12</sup>A. Ghizzo, D. Del Sarto, F. Palermo, and A. Biancalani, "Transport barriers associated to the resonant interaction between trapped particle modes triggered by plasma polarization injection," *EPL* **119**, 15003 (2017).
- <sup>13</sup>L. Chen, Z. Lin, and R. White, "Excitation of zonal flow by drift waves in toroidal plasmas," *Phys. Plasmas* **7**, 3129–3132 (2000).
- <sup>14</sup>P. G. Ivanov, A. A. Schekochihin, and W. Dorland, "Dimits transition in three-dimensional ion-temperature-gradient turbulence," *J. Plasma Phys.* **88**, 905880506 (2022).
- <sup>15</sup>N. Miyato, J. Li, and Y. Kishimoto, "Study of a drift wave-zonal mode system based on global electromagnetic Landau-fluid ITG simulation in toroidal plasmas," *Nucl. Fusion* **45**, 425 (2005).
- <sup>16</sup>Z. Qiu, L. Chen, and F. Zonca, "Nonlinear excitation of finite-radial-scale zonal structures by toroidal Alfvén eigenmode," *Nucl. Fusion* **57**, 056017 (2017).
- <sup>17</sup>A. Biancalani, A. Bottino, S. Brunner, A. Di Siena, T. Görler, R. Hatzky, F. Jenko, A. Könies, P. Lauber, I. Novikau *et al.*, "Interaction of Alfvénic modes and turbulence, investigated in a self-consistent gyrokinetic framework," in 46th EPS Conference on Plasma Physics, I5J602 (2019).
- <sup>18</sup>F. Wagner, G. Fussmann, T. Grave, M. Keilhacker, M. Kornherr, K. Lackner, K. McCormick, E. R. Müller, A. Stäbler, G. Becker, K. Bernhardt, U. Ditte, A. Eberhagen, O. Gehre, J. Gernhardt, G. v. Gierke, E. Glock, O. Gruber, G. Haas, M. Hesse, G. Janeschitz, F. Karger, S. Kissel, O. Klüber, G. Lisitano, H. M. Mayer, D. Meisel, V. Mertens, H. Murmann, W. Poschenrieder, H. Rapp, H. Röhr, F. Rytter, F. Schneider, G. Siller, P. Smeulders, F. Söldner, E. Speth, K. H. Steuer, Z. Szymanski, and O. Vollmer, "Development of an edge transport barrier at the h-mode transition of ASDEX," *Phys. Rev. Lett.* **53**, 1453–1456 (1984).
- <sup>19</sup>R. Wolf, "Internal transport barriers in tokamak plasmas," *Plasma Phys. Control. Fusion* **45**, R1 (2003).
- <sup>20</sup>J. Citrin, F. Jenko, P. Mantica, D. Told, C. Bourdelle, J. Garcia, J. W. Haverkort, G. M. D. Hogewijj, T. Johnson, and M. J. Pueschel, "Nonlinear stabilization of tokamak microturbulence by fast ions," *Phys. Rev. Lett.* **111**, 155001 (2013).
- <sup>21</sup>M. Romanelli, A. Zocco, and F. Crisanti, and JET-EFDA Contributors, "Fast ion stabilization of the ion temperature gradient driven modes in the joint European torus hybrid-scenario plasmas: A trigger mechanism for internal transport barrier formation," *Plasma Phys. Control. Fusion* **52**, 045007 (2010).
- <sup>22</sup>G. Tardini, J. Hobirk, V. Igochine, C. Maggi, P. Martin, D. McCune, A. Peeters, A. Sips, A. Stäbler, and J. Stober, and the ASDEX Upgrade Team, "Thermal ions dilution and ITG suppression in ASDEX upgrade ion ITBS," *Nucl. Fusion* **47**, 280 (2007).
- <sup>23</sup>A. Di Siena, T. Görler, H. Doerk, E. Poli, and R. Bilato, "Fast-ion stabilization of tokamak plasma turbulence," *Nucl. Fusion* **58**, 054002 (2018).
- <sup>24</sup>A. Di Siena, R. Bilato, T. Görler, A. Bañón Navarro, E. Poli, V. Bobkov, D. Jarema, E. Fable, C. Angioni, Y. O. Kazakov *et al.*, "New high-confinement regime with fast ions in the core of fusion plasmas," *Phys. Rev. Lett.* **127**, 025002 (2021).
- <sup>25</sup>S. Mazzi, J. Garcia, D. Zarzoso, Y. O. Kazakov, J. Ongena, M. Dreval, M. Nocente, Ž. Stancar, G. Szepesi, J. Eriksson *et al.*, "Enhanced performance in fusion plasmas through turbulence suppression by megaelectronvolt ions," *Nat. Phys.* **18**, 776–782 (2022).
- <sup>26</sup>J. Garcia and JET Contributors, "Electromagnetic and fast ions effects as a key mechanism for turbulent transport suppression at jet," *Plasma Phys. Control. Fusion* **64**, 104002 (2022).
- <sup>27</sup>G. J. Wilkie, I. Pusztai, I. Abel, W. Dorland, and T. Fülöp, "Global anomalous transport of ICRH- and NBI-heated fast ions," *Plasma Phys. Control. Fusion* **59**, 044007 (2017).
- <sup>28</sup>N. Bonanomi, P. Mantica, A. Di Siena, E. Delabie, C. Giroud, T. Johnson, E. Lerche, S. Menmuir, M. Tsalas, D. Van Eester *et al.*, "Turbulent transport stabilization by ICRH minority fast ions in low rotating jet ILW L-mode plasmas," *Nucl. Fusion* **58**, 056025 (2018).
- <sup>29</sup>A. Di Siena, T. Görler, E. Poli, R. Bilato, H. Doerk, and A. Zocco, "Resonant interaction of energetic ions with bulk-ion plasma micro-turbulence," *Phys. Plasmas* **26**, 052504 (2019).
- <sup>30</sup>P. Mantica, D. Stryntzi, T. Tala, C. Giroud, T. Johnson, H. Leggate, E. Lerche, T. Loarer, A. Peeters, A. Salmi *et al.*, "Experimental study of the ion critical-gradient length and stiffness level and the impact of rotation in the jet tokamak," *Phys. Rev. Lett.* **102**, 175002 (2009).
- <sup>31</sup>P. Mantica, C. Angioni, C. Challis, G. Colyer, L. Frassinetti, N. Hawkes, T. Johnson, M. Tsalas, P. Devries, J. Weiland *et al.*, "A key to improved ion core confinement in the jet tokamak: Ion stiffness mitigation due to combined plasma rotation and low magnetic shear," *Phys. Rev. Lett.* **107**, 135004 (2011).
- <sup>32</sup>J. Citrin and P. Mantica, "Overview of tokamak turbulence stabilization by fast ions," *Plasma Phys. Control. Fusion* **65**(3), 033001 (2023).
- <sup>33</sup>G. Whelan, M. Pueschel, and P. Terry, "Nonlinear electromagnetic stabilization of plasma microturbulence," *Phys. Rev. Lett.* **120**, 175002 (2018).
- <sup>34</sup>A. Di Siena, T. Görler, E. Poli, A. Bañón Navarro, A. Biancalani, and F. Jenko, "Electromagnetic turbulence suppression by energetic particle driven modes," *Nucl. Fusion* **59**, 124001 (2019b).
- <sup>35</sup>J. Citrin, J. Garcia, T. Görler, F. Jenko, P. Mantica, D. Told, C. Bourdelle, D. Hatch, G. Hogewijj, T. Johnson *et al.*, "Electromagnetic stabilization of tokamak microturbulence in a high- $\beta$  regime," *Plasma Phys. Control. Fusion* **57**, 014032 (2015).
- <sup>36</sup>A. Di Siena, T. Hayward-Schneider, P. Mantica, J. Citrin, F. Vannini, A. Bottino, T. Görler, E. Poli, R. Bilato, O. Sauter *et al.*, "How accurate are flux-tube (local) gyrokinetic codes in modelling energetic particle effects on core turbulence?," *Nucl. Fusion* **63**, 106012 (2023).
- <sup>37</sup>M. Nocente, Y. O. Kazakov, J. Garcia, V. Kiptily, J. Ongena, M. Dreval, M. Fitzgerald, S. E. Sharapov, Z. Stancar, H. Weisen *et al.*, "Generation and observation of fast deuterium ions and fusion-born alpha particles in jet plasmas with the 3-ion radio-frequency heating scenario," *Nucl. Fusion* **60**, 124006 (2020).
- <sup>38</sup>Y. O. Kazakov, M. Nocente, M. Mantsinen, J. Ongena, Y. Baranov, T. Craciunescu, M. Dreval, R. Dumont, J. Eriksson, J. Garcia *et al.*, "Plasma

- heating and generation of energetic d ions with the 3-ion ICRF+NBI scenario in mixed HD plasmas at jet-ILW," *Nucl. Fusion* **60**, 112013 (2020).
- <sup>39</sup>R. B. White and H. E. Mynick, "Alpha particle confinement in tokamaks," *Phys. Fluids B* **1**, 980–982 (1989).
- <sup>40</sup>F. Zonca, L. Chen, S. Briguglio, G. Fogaccia, A. V. Milovanov, Z. Qiu, G. Vlad, and X. Wang, "Energetic particles and multi-scale dynamics in fusion plasmas," *Plasma Phys. Control. Fusion* **57**, 014024 (2015).
- <sup>41</sup>N. Chen, H. Hu, X. Zhang, S. Wei, and Z. Qiu, "Effects of radial electric field on ion temperature gradient driven mode stability," *Phys. Plasmas* **28**, 042505 (2021).
- <sup>42</sup>T. S. Hahm, G. J. Choi, S. J. Park, and Y.-S. Na, "Fast ion effects on zonal flow generation: A simple model," *Phys. Plasmas* **30**, 072501 (2023).
- <sup>43</sup>A. Ghizzo and D. Del Sarto, "Low-frequency turbulence suppression by amplification of synchronized zonal flow with energetic particle driven modes," *Nucl. Fusion* **63**, 104002 (2023).
- <sup>44</sup>C. Angioni, A. Peeters, G. Pereverzev, A. Bottino, J. Candy, R. Dux, E. Fable, T. Hein, and R. Waltz, "Gyrokinetic simulations of impurity, the ash and  $\alpha$  particle transport and consequences on ITER transport modelling," *Nucl. Fusion* **49**, 055013 (2009).
- <sup>45</sup>E. M. Bass and R. E. Waltz, "Gyrokinetic simulations of mesoscale energetic particle-driven Alfvénic turbulent transport embedded in microturbulence," *Phys. Plasmas* **17**, 112319 (2010).
- <sup>46</sup>W. Zhang, V. Decyk, I. Holod, Y. Xiao, Z. Lin, and L. Chen, "Scalings of energetic particle transport by ion temperature gradient microturbulence," *Phys. Plasmas* **17**, 055902 (2010).
- <sup>47</sup>J. Garcia, C. Challis, J. Citrin, H. Doerk, G. Giruzzi, T. Görler, F. Jenko, P. Maget, and J. Contributors, "Key impact of finite-beta and fast ions in core and edge tokamak regions for the transition to advanced scenarios," *Nucl. Fusion* **55**, 053007 (2015).
- <sup>48</sup>K. Appert, R. Gruber, F. Troyon, and J. Vaclavik, "Excitation of global eigenmodes of the Alfvén wave in tokamaks," *Plasma Phys.* **24**, 1147 (1982).
- <sup>49</sup>L. Chen and F. Zonca, "Physics of Alfvén waves and energetic particles in burning plasmas," *Rev. Mod. Phys.* **88**, 015008 (2016).
- <sup>50</sup>Y. Todo, H. Berk, and B. Breizman, "Nonlinear magnetohydrodynamic effects on Alfvén eigenmode evolution and zonal flow generation," *Nucl. Fusion* **50**, 084016 (2010).
- <sup>51</sup>A. Mishchenko, A. Bottino, A. Biancalani, R. Hatzky, T. Hayward-Schneider, N. Ohana, E. Lanti, S. Brunner, L. Villard, M. Borchardt, R. Kleiber, and A. Könies, "Pullback scheme implementation in ORB5," *Comput. Phys. Commun.* **238**, 194–202 (2019).
- <sup>52</sup>E. Lanti, N. Ohana, N. Tronko, T. Hayward-Schneider, A. Bottino, B. McMillan, A. Mishchenko, A. Scheinberg, A. Biancalani, P. Angelino, S. Brunner, J. Dominski, P. Donnel, C. Gheller, R. Hatzky, A. Jocksch, S. Joliet, Z. Lu, J. Martin Collar, I. Novikau, E. Sonnendrücker, T. Vernay, and L. Villard, "ORB5: A global electromagnetic gyrokinetic code using the pic approach in toroidal geometry," *Comput. Phys. Commun.* **251**, 107072 (2020).
- <sup>53</sup>A. Biancalani, A. Bottino, D. Del Sarto, M. Falessi, T. Hayward-Schneider, P. Lauber, A. Mishchenko, B. Rettino, J. Sama, F. Vannini *et al.*, "Nonlinear interaction of Alfvénic instabilities and turbulence via the modification of the equilibrium profiles," *J. Plasma Phys.* **89**, 905890602 (2023).
- <sup>54</sup>A. Di Siena, T. Görler, E. Poli, A. Bañón Navarro, A. Biancalani, and F. Jenko, "Electromagnetic turbulence suppression by energetic particle driven modes," *Nucl. Fusion* **59**, 124001 (2019).
- <sup>55</sup>A. Ishizawa, K. Imadera, Y. Nakamura, and Y. Kishimoto, "Multi-scale interactions between turbulence and magnetohydrodynamic instability driven by energetic particles," *Nucl. Fusion* **61**, 114002 (2021).
- <sup>56</sup>J. Conner and H. Wilson, "Survey of theories of anomalous transport," *Plasma Phys. Control. Fusion* **36**, 719 (1994).
- <sup>57</sup>K. Miyamoto, *Plasma Physics and Controlled Nuclear Fusion* (Springer Science & Business Media, 2005), Vol. 38.
- <sup>58</sup>S. Joliet, A. Bottino, P. Angelino, R. Hatzky, T.-M. Tran, B. Mcmillan, O. Sauter, K. Appert, Y. Idomura, and L. Villard, "A global collisionless PIC code in magnetic coordinates," *Comput. Phys. Commun.* **177**, 409–425 (2007).
- <sup>59</sup>A. Mishchenko, A. Biancalani, A. Bottino, T. Hayward-Schneider, P. Lauber, E. Lanti, L. Villard, R. Kleiber, A. Könies, and M. Borchardt, "Numerics and computation in gyrokinetic simulations of electromagnetic turbulence with global particle-in-cell codes," *Plasma Phys. Control. Fusion* **63**, 084007 (2021).
- <sup>60</sup>R. J. Dumont, J. Mailloux, V. Aslanyan, M. Baruzzo, C. Challis, I. Coffey, A. Czarnecka, E. Delabie, J. Eriksson, J. Faustin, J. Ferreira, M. Fitzgerald, J. Garcia, L. Giacomelli, C. Giroud, N. Hawkes, P. Jacquet, E. Joffrin, T. Johnson, D. Keeling, D. King, V. Kiptily, B. Lomanowski, E. Lerche, M. Mantsinen, L. Meneses, S. Menmuir, K. McClements, S. Moradi, F. Nabais, M. Nocente, A. Patel, H. Patten, P. Puglia, R. Scannell, S. Sharapov, E. R. Solano, M. Tsalas, P. Vallejos, and H. Weisen, and J. Contributors, "Scenario development for the observation of alpha-driven instabilities in jet DT plasmas," *Nucl. Fusion* **58**, 082005 (2018).
- <sup>61</sup>M. Fitzgerald, S. Sharapov, P. Siren, E. Tholerus, M. Dreval, G. Szepesi, P. Vallejos, T. Johnson, N. Fil, J. Ferreira, P. Rodrigues, A. Figueiredo, D. Borba, R. Coelho, F. Nabais, J. Mailloux, H. Oliver, C. D. Troia, F. Napoli, Z. Stancar, R. Dumont, and D. Keeling, and J. Contributors, "Toroidal Alfvén eigenmode stability in jet internal transport barrier afterglow experiments," *Nucl. Fusion* **62**, 106001 (2022).
- <sup>62</sup>G. T. A. Huysmans, S. E. Sharapov, A. B. Mikhailovskii, and W. Kerner, "Modeling of diamagnetic stabilization of ideal magnetohydrodynamic instabilities associated with the transport barrier," *Phys. Plasmas* **8**, 4292–4305 (2001).
- <sup>63</sup>H. Lütjens, A. Bondeson, and O. Sauter, "The CHEASE code for toroidal MHD equilibria," *Comput. Phys. Commun.* **97**, 219–260 (1996).
- <sup>64</sup>M. Podestá, M. Gorelenkova, and R. B. White, "A reduced fast ion transport model for the tokamak transport code TRANSP," *Plasma Phys. Control. Fusion* **56**, 055003 (2014).
- <sup>65</sup>H. L. Berk, J. W. Van Dam, Z. Guo, and D. M. Lindberg, "Continuum damping of low-n toroidicity-induced shear Alfvén eigenmodes," *Phys. Fluids B* **4**, 1806–1835 (1992).
- <sup>66</sup>M. V. Falessi, N. Carlevaro, V. Fusco, E. Giovannozzi, P. Lauber, G. Vlad, and F. Zonca, "On the polarization of shear Alfvén and acoustic continuous spectra in toroidal plasmas," *J. Plasma Phys.* **86**, 845860501 (2020).
- <sup>67</sup>Z. Qiu, L. Chen, and F. Zonca, "Gyrokinetic theory of toroidal Alfvén eigenmode saturation via nonlinear wave-wave coupling," *Rev. Mod. Plasma Phys.* **7**, 28 (2023).
- <sup>68</sup>K. Crombé, Y. Andrew, T. M. Biewer, E. Blanco, P. C. de Vries, C. Giroud, N. C. Hawkes, A. Meigs, T. Tala, M. von Hellermann, K.-D. Zastrow, and J. E. Contributors, "Radial electric field in jet advanced tokamak scenarios with toroidal field ripple," *Plasma Phys. Control. Fusion* **51**, 055005 (2009).
- <sup>69</sup>N. Ohana, L. Villard, E. Lanti, S. Brunner, B. F. McMillan, N. Tronko, A. Bottino, A. Biancalani, I. Novikau, and A. Mishchenko, "Mode excitation by an antenna in global gyrokinetic simulations," *J. Phys. Conf. Ser.* **1125**, 012017 (2018).
- <sup>70</sup>M. Sadr, A. Mishchenko, T. Hayward-Schneider, A. Koenies, A. Bottino, A. Biancalani, P. Donnel, E. Lanti, and L. Villard, "Linear and nonlinear excitation of TAE modes by external electromagnetic perturbations using ORB5," *Plasma Phys. Control. Fusion* **64**, 085010 (2022).
- <sup>71</sup>S. J. Allfrey, A. Bottino, O. Sauter, and L. Villard, "The role of radial electric fields in linear and nonlinear gyrokinetic full radius simulations," *New J. Phys.* **4**, 29 (2002).
- <sup>72</sup>A. Biancalani, A. Bottino, A. D. Siena, Ö. Gürçan, T. Hayward-Schneider, F. Jenko, P. Lauber, A. Mishchenko, P. Morel, I. Novikau, F. Vannini, L. Villard, and A. Zocco, "Gyrokinetic investigation of Alfvén instabilities in the presence of turbulence," *Plasma Phys. Control. Fusion* **63**, 065009 (2021).